

Journal of Medicinal Chemistry

Subscriber access provided by UNIVERSITA STUDI TRIESTE

Article

Peptide inhibitors of bacterial protein synthesis with broad spectrum and SbmA-independent bactericidal activity against clinical pathogens.

Mario Mardirossian, Riccardo Sola, Bertrand Beckert, Erica Valencic, Dominic W. P. Collis, Jure Borišek, Federica Armas, Adriana Di Stasi, Jan Buchmann, Egor A. Syroegin, Yury Polikanov, Alessandra Magistrato, Kai Hilpert, Daniel N. Wilson, and Marco Scocchi

J. Med. Chem., **Just Accepted Manuscript** • DOI: 10.1021/acs.jmedchem.0c00665 • Publication Date (Web): 29 Jul 2020

Downloaded from pubs.acs.org on August 3, 2020

Just Accepted

“Just Accepted” manuscripts have been peer-reviewed and accepted for publication. They are posted online prior to technical editing, formatting for publication and author proofing. The American Chemical Society provides “Just Accepted” as a service to the research community to expedite the dissemination of scientific material as soon as possible after acceptance. “Just Accepted” manuscripts appear in full in PDF format accompanied by an HTML abstract. “Just Accepted” manuscripts have been fully peer reviewed, but should not be considered the official version of record. They are citable by the Digital Object Identifier (DOI®). “Just Accepted” is an optional service offered to authors. Therefore, the “Just Accepted” Web site may not include all articles that will be published in the journal. After a manuscript is technically edited and formatted, it will be removed from the “Just Accepted” Web site and published as an ASAP article. Note that technical editing may introduce minor changes to the manuscript text and/or graphics which could affect content, and all legal disclaimers and ethical guidelines that apply to the journal pertain. ACS cannot be held responsible for errors or consequences arising from the use of information contained in these “Just Accepted” manuscripts.

1
2
3
4 **1 Peptide inhibitors of bacterial protein synthesis with broad spectrum and**
5
6
7 **2 SbmA-independent bactericidal activity against clinical pathogens.**
8
9

10 **3 Mario Mardirossian¹, Riccardo Sola², Bertrand Beckert³, Erica Valencic⁴, Dominic W. P.**
11
12 **4 Collis⁵, Jure Borišek⁶, Federica Armas², Adriana Di Stasi², Jan Buchmann^{3,7}, Egor A.**
13
14 **5 Syroegin⁷, Yury S. Polikanov^{7,8}, Alessandra Magistrato⁶, Kai Hilpert⁹, Daniel N. Wilson³,**
15
16
17 **6 Marco Scocchi^{2*}.**
18
19

20 **7** ¹ Department of Medical Sciences, University of Trieste, 34125 Trieste, Italy.
21
22

23 **8** ² Department of Life Sciences, University of Trieste, 34127 Trieste, Italy.
24
25

26 **9** ³ Institut für Biochemie und Molekularbiologie, University of Hamburg, 20146 Hamburg,
27
28 **10** Germany.
29
30

31 **11** ⁴ Institute for Maternal and Child Health-IRCCS "Burlo Garofolo", 30137 Trieste, Italy.
32
33

34 **12** ⁵ TiKa Diagnostics Ltd, SW 17 ORE London, UK.
35
36

37 **13** ⁶ CNR-IOM at SISSA, 34136 Trieste, Italy.
38
39

40 **14** ⁷ Department of Biological Sciences, University of Illinois at Chicago, Chicago, IL 60607, USA.
41
42

43 **15** ⁸ Department of Pharmaceutical Sciences, University of Illinois at Chicago, Chicago, IL 60607,
44
45 **16** USA.
46

47 **17** ⁹ Institute of Infection and Immunology, St. George's, University of London, SW 17 ORE London,
48
49 **18** UK.
50
51

1
2
3 **22 Abstract**
4
5

6 23 Proline-rich antimicrobial peptides (PrAMPs) are promising lead compounds for developing new
7
8 24 antimicrobials, however their narrow spectrum of action is limiting. PrAMPs kill bacteria binding to
9
10 25 their ribosomes and inhibiting protein synthesis. In this study, 133 derivatives of the PrAMP
11
12 26 Bac7(1-16) were synthesized to identify the crucial residues for ribosome inactivation and
13
14 27 antimicrobial activity. Then, five new Bac7(1-16) derivatives were conceived and characterized by
15
16 28 antibacterial and membrane permeabilization assays, by X-ray crystallography and molecular
17
18 29 dynamics simulations. Some derivatives displayed broad spectrum activity, encompassing
19
20 30 *Escherichia coli*, *Klebsiella pneumoniae*, *Acinetobacter baumannii*, *Pseudomonas aeruginosa* and
21
22 31 *Staphylococcus aureus*. Two peptides out of five, acquired a weak membrane-perturbing activity,
23
24 32 while maintaining the ability to inhibit protein synthesis. These derivatives became independent of
25
26 33 the SbmA transporter, commonly used by native PrAMPs, suggesting that they obtained a novel
27
28 34 route to enter bacterial cells. PrAMP-derived compounds could become new-generation
29
30 35 antimicrobials to combat the antibiotic-resistant pathogens.
31
32
33
34
35
36
37 36
38
39
40 37
41
42
43 38
44
45
46 39
47
48
49 40
50
51
52 41
53
54
55 42
56
57
58 43
59
60

1 Introduction

2 The search for new antimicrobial agents is propelled by the continuous emergence of
3 antibiotic-resistant pathogens ¹. In the recent years, there has been increasing interest in testing
4 antimicrobial peptides (AMPs) as lead compounds for the development of new antibiotics ².
5 Proline-rich antimicrobial peptides (PrAMPs) are particularly promising as they combine potent
6 antimicrobial activity with low toxicity toward eukaryotic cells ³, a feature owing to their non-lytic
7 mode of action ⁴. PrAMPs do not permeabilize the bacterial membranes ⁴, but rather they enter the
8 cells of several Gram-negative species (e.g. *Enterobacteriaceae*) by active transport, using
9 predominantly the bacterial inner membrane transporter SbmA ^{3, 5-7}. Once inside the bacterial cell,
10 PrAMPs kill bacteria by binding to their ribosomes and inhibiting protein synthesis ⁸⁻¹⁰. Two
11 distinct mechanisms of action have so far been described in molecular details for different PrAMPs:
12 (i) type I PrAMPs allow initiation of protein synthesis, but prevent the transition into the elongation
13 phase by impeding the accommodation of the first aminoacyl-tRNA ¹¹⁻¹⁶, whereas (ii) type II
14 PrAMPs allow initiation and elongation of protein synthesis, but interfere with translation
15 termination by trapping the release factors on the ribosome^{17, 18}. Interestingly, inhibition of bacterial
16 protein synthesis is a feature shared by PrAMPs present in phylogenetically-distinct organisms,
17 such as insects (apidaecins and oncocins) and mammals (Bac7 and Bac5 derivatives, as well as
18 Tur1A), most probably as a result of convergent evolution ³. The distinctive mode of transport of
19 PrAMPs into bacterial cells using the bacterial membrane protein SbmA makes PrAMP activity
20 strongly dependent on the presence of this transporter, thus limiting their spectrum of activity
21 mainly to those pathogens that express SbmA ³.

22 During the recent years, some mammalian and insect PrAMPs were subjected to systematic
23 sequence and length modifications with the aim of improving their antimicrobial potential, their
24 spectrum of activity as well as of reducing the cost of manufacturing ¹⁹⁻²⁴. Peptide libraries designed
25 on the insect-derived apidaecin ^{19, 25} and oncocin ^{20, 26} were synthesized by SPOT synthesis and

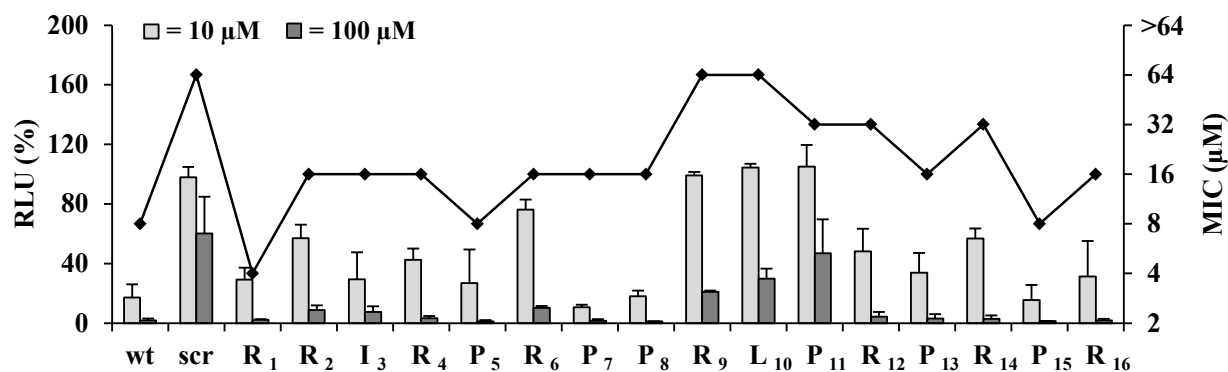
1
2
3 26 tested for their antimicrobial effect. Some of these variants were identified with improved
4
5 27 antimicrobial activity against pathogens, such as *Pseudomonas aeruginosa*, *Staphylococcus aureus*
6
7
8 28 and *Escherichia coli*. A similar approach was applied to a derivative of the mammalian PrAMP
9
10 29 Bac5(1-17) resulting in peptides with improved antimicrobial effect against *E. coli*, *Klebsiella*
11
12 30 *pneumoniae* and *Acinetobacter baumannii*²². N-terminal fragments of the native mammalian
13
14 31 PrAMPs Bac7²⁷ are among the best characterized mammalian PrAMPs, however their systematic
15
16
17 32 modification to identify new derivatives with improved antimicrobial properties is still embryonic
18
19 33 ^{21, 28} and deserves further and broader efforts.

21
22 34 In this work we systematically modified Bac7(1-16) to identify the amino acid residues that
23
24 35 are essential for the ribosome binding and antimicrobial activity. These data were then used to
25
26
27 36 direct the design of novel derivatives with increasing antimicrobial properties. Five derivatives were
28
29 37 conceived and analysed for their activity and mechanism of action. X-ray crystallography and
30
31 38 molecular dynamics simulations^{29, 30} were then employed to obtain structural insights into the
32
33
34 39 binding mode of these peptides with their target. Our results reveal that residues Arg₉-Arg₁₂ of
35
36 40 Bac7(1-16) are crucial for the inhibition of bacterial growth and protein synthesis. The introduction
37
38 41 of Arg and Trp residues in specific positions of the peptide's sequence modified the mode of some
39
40 42 derivatives to enter bacteria and promoted their antimicrobial activity against a broadened spectrum
41
42
43 43 of bacterial pathogens. These data provide new insights for the rational design of more potent
44
45 44 antimicrobial drugs, which are urgently needed to fight the growing tide of antibiotic-resistant
46
47
48 45 bacterial infections.

47 Results

48 Identification of Bac7(1-16) residues essential for the inhibition of protein synthesis

49 To identify the residues of Bac7(1-16) essential for antimicrobial activity, a library of 16
 50 peptides was prepared where each residue was individually replaced by alanine. The antimicrobial
 51 activity and the protein synthesis-inhibiting activity of the modified peptides were assessed by
 52 determination of the minimum inhibitory concentration (MIC) as well as using an *in vitro*
 53 transcription/translation assay, respectively (**Fig. 1**). The substitution of any residue in the ${}_{9}\text{RLP}_{11}$
 54 portion of the Bac7(1-16) dramatically reduced its potential to inhibit both bacterial protein
 55 synthesis as well as the growth of *E. coli* cells. Amino acid substitutions in other regions were better
 56 tolerated, and the replacement of Arg1 with Ala (R1A) was even a beneficial change, improving the
 57 antimicrobial activity of the peptide. The similar trend between the MICs and the inhibition of the
 58 transcription/translation suggested that changes in antimicrobial activity of the peptide variants
 59 were mainly due to a corresponding change in the inhibitory activity on protein synthesis.



60

61

62

63

64

65

66

67

68

69

70

71

72

73

74

75

76

77

78

Figure 1. Luminescence after *in vitro* transcription/translation using *E. coli* lysates (histograms) and MIC values on *E. coli* cells (black line) in the presence of Bac7(1-16) alanine-substituted variants. The peptide sequence is displayed on the x-axis. The values above each residue refer to the peptide carrying the alanine substitution in that position. Unmodified (wt) and scrambled (scr) peptides were used as controls. Transcription/translation reactions (left y-axis) were performed in presence of 10 μM (light grey) and 100 μM (dark grey) peptide. Luminescence of the

1
2
3 67 translated luciferase was normalized using the untreated controls (RLU%). Error bars indicate the
4
5 68 standard deviation calculated on the mean of at least two independent experiments. MIC values
6
7
8 69 (right y-axis and black line) against *E. coli* BW25113 are the median calculated on at least three
9
10 70 independent experiments

11
12
13 71

16 72 **Activity of Bac7(1-16) variants bearing diverse amino acid substitutions**

19 73 To identify novel Bac7(1-16) derivatives with improved antimicrobial activity with respect
20
21 74 to the original Bac7(1-16) peptide, a new peptide library (114 members) was prepared by SPOT-
22
23
24 75 synthesis. Each Bac7(1-16) residue was substituted with either glycine, alanine or serine (absent,
25
26 76 short non-polar or polar side chain, respectively), proline (secondary structure disrupting-residue),
27
28 77 arginine or glutamic acid (long basic or acidic side chain), phenylalanine or tryptophan (bulky
29
30 78 aromatic side chain). All members of this peptide library were then tested by MIC assays in full
31
32
33 79 Müller-Hinton medium on *E. coli* BW25113 (**Table 1**). In 61.6% of the substitutions only a small
34
35 80 change in the MIC values was measured (2-fold change compared to wild type) (**Table S1**). R1W
36
37 81 and P13W substitutions, representing 1.8% of all the peptides, showed a 4-fold improvement in the
38
39 82 MIC values (MIC = 2 μ M). In 31.1% of the substitutions the MIC values dropped to 4-8-fold and
40
41
42 83 4.4% showed no activity at the highest concentration measured (64 μ M). The position R9, L10,
43
44 84 P11, R12 and R14 showed the least amount of tolerance to substitutions, with most of the
45
46 85 substitutions showing a medium to strong decrease in antimicrobial activity (**Table S1**). Most
47
48 86 substitutions with Gly (G), Ala (A), Ser (S) and Pro (P) led to a decreased antibacterial effect. The
49
50 87 substitution with Glu (E) was always adverse, leading to inactivation of the peptide regardless of the
51
52 88 position (MICs 32- \rightarrow 64 μ M), similar to the effect of the scrambled peptide used as a control (**Table**
53
54 89 **1**). This result was not surprising given that the binding of Bac7(1-16) with the ribosome involves
55
56 90 several arginines that form hydrogen bonds with nucleotides of the 23S rRNA, as well as
57
58 91 electrostatic interactions with its phosphate groups¹¹. In contrast, amino acid substitutions with Arg

1
2
3 92 (R), Phe (F) or Trp (W) were well tolerated resulting in unchanged or improved antimicrobial
4
5 93 activity (**Table 1**). This result was consistent with the general binding mode proposed for PrAMPs
6
7
8 94 on the ribosome where the side chains of arginines and aromatic residues establish multiple stacking
9
10 95 interactions with the rRNA ¹¹.

11
12
13 96 **Table 1.** MIC values (μM) against *E. coli* BW25113 of the wild-type Bac7(1-16) compared with
14
15 97 scrambled and substituted variants.

16
17
18
19
20
21
22
23
24
25
26
27
28
29
30
31
32
33
34
35
36
37
38
39
40
41
42
43
44
45
46
47
48
49

Bac7 (1-16) ^a	MIC (μM)									
	wt ^b	scr ^c	G	A ^d	S	P	R	E	F	W
R ₁	8	64	8	4	16	8	-	64	4	2
R ₂			16	16	16	64	-	64	16	8
I ₃			16	16	16	16	8	64	16	4
R ₄			16	16	32	16	-	>64	16	8
P ₅			8	8	16	-	8	32	8	4
R ₆			32	16	32	32	-	>64	16	8
P ₇			16	16	16	-	8	32	8	4
P ₈			16	16	16	-	16	64	16	4
R ₉			64	64	32	16	-	>64	16	4
L ₁₀			64	64	32	64	32	>64	32	16
P ₁₁			32	32	32	-	16	64	32	8
R ₁₂			32	32	16	32	-	>64	16	8
P ₁₃			16	16	16	-	8	64	8	2
R ₁₄			32	32	32	32	-	64	8	4
P ₁₅			16	8	16	-	16	32	8	4
R ₁₆			16	16	16	32	-	64	8	8

50 98 Substitutions improving antimicrobial activity compared to the native Bac5(1-17) are highlighted in grey shades;

51
52 99 ^aBac7(1-16) sequence and position numbers; ^bBac7(1-16) wild-type; ^cBac7(1-16) scrambled: IRPLPPRRPRRRPRR. ^d

53
54 100 For comparison the Ala-scan MIC values from Figure 1 are also included in this table. Results are reported as median of
55
56 101 at least three independent experiments ($n \geq 3$).

57
58 102
59
60

1
2
3 103 **Antimicrobial activity and bio-compatibility of mono- and multi-substituted Bac7(1-16)**
4
5 104 **derivatives.**
6
7

8
9 105 Introduction of different Arg and Trp residues, which singularly often increased
10
11 106 antimicrobial activity of Bac7(1-16) (**Table 1**), were combined to design new Bac7(1-16) multi-
12
13 107 substituted derivatives. Two positions within the Bac7(1-16) peptide, namely R1 and P13, when
14
15 108 substituted by (W) led to the best activity improvements (2 μ M, **Table 1**). We combined these
16
17 109 modifications to produce the di-substituted Bac7(1-16) derivative B7-003 (**Table 2**). We then tried
18
19 110 different substitutions to generate the tri- and tetra-substituted Bac7(1-16) derivatives B7-004 and
20
21 111 B7-005 (**Table 2**). These derivatives displayed an R, W and W residues at position P5, P7, and P15
22
23 112 respectively, where also the substitution with other amino acids (namely, G, A, R, F for P5; R, F for
24
25 113 P7; and A, F for P15) was well-tolerated. These five derivatives were synthesized on resin by solid-
26
27 114 phase and highly purified (purity \geq 95%) together with the wild-type Bac7(1-16) as a control. B7-
28
29 115 001 and B7-002, which were the most active single substituted peptides bearing the substitution as
30
31 116 far as possible from the critical R₉-P₁₁ residues, were also synthesised (**Table 2**).
32
33

34 117 All these highly-purified peptides displayed a MIC of 1-2 μ M against *E. coli* BW25113 and
35
36 118 *E. coli* ATCC 25922 (**Table 2**). None of the multi-substituted peptides possessed a higher
37
38 119 antimicrobial activity than the wild-type Bac7(1-16) or the mono-substituted B7-001 and B7-002.
39
40 120 The lower MIC value against *E. coli* BW25113 observed for the purified Bac7(1-16) (2 μ M) with
41
42 121 respect to that obtained by SPOT-synthesis (8 μ M) may be due to lower purity level resulting from
43
44 122 the SPOT-synthesis technique. We simultaneously determined whether the Bac7(1-16) derivatives
45
46 123 exhibited differential susceptibility to degradation by blood serum proteases compared to the native
47
48 124 Bac7(1-16), and thereby if they lose their antimicrobial properties. MIC assays carried out using the
49
50 125 *E. coli* reference strain ATCC 25922 indicated that peptides B7-001, B7-002 and B7-003, as well as
51
52 126 the wild-type Bac7(1-16) were fully active in the presence of serum (**Table 2**). On the other hand,
53
54 127 3- and 6-fold MIC increase was observed for B7-004 and B7-005, respectively. This result
55
56 128 suggested that insertion of multiple W and/or R residues in the sequence might increase the
57
58
59
60

1
2
3 129 susceptibility of the peptides to protease degradation. In parallel, the biocompatibility of Bac7(1-16)
4
5 130 derivatives was evaluated using the human leukaemia cell line MEC-1. Importantly, none of them
6
7
8 131 displayed any significant toxicity, even at 64 μM after 24 hours of exposure (**Table 2** and **Fig. S1**),
9

10
11 132 **Table 2.** Antimicrobial activity in absence or presence of serum and cytotoxicity of
12
13 133 purified Bac7(1-16) derivatives.
14

B7-code	Sequence	MIC on <i>E. coli</i> (μM)			Cytotox ^c (μM)
		BW25113	ATCC 25922	ATCC 25922+ser ^b	
wt ^a	RRIRPRPPRLPRPRPR	2	1	1	>64
001	<u>W</u> RRIRPRPPRLPRPRPR	1	1	1	>64
002	RRIRPRPPRLPRPR <u>W</u> R	1	1	1.5	>64
003	<u>W</u> RRIRPRPPRLPR <u>W</u> RPR	2	1.5	2	>64
004	<u>W</u> RRIR <u>R</u> RPPRLPRPR <u>W</u> R	1	1	6	>64
005	<u>W</u> RRIR <u>R</u> <u>W</u> PPRLPRPR <u>W</u> R	2	1	3	>64

15
16
17
18
19
20
21
22
23
24
25
26
27
28
29
30
31
32 134 Results are the median of at least three independent experiments (n=3), ^awt = wild-type Bac7(1-16),
33
34 135 ^bser= 10% (v/v) human serum in full MH medium, ^cCytotox= p-value ≤ 0.05 , Student t-test, peptide-
35
36 136 treated MEC-1 cells VS untreated control.
37

38 137

39 138

40 41 139 **Broader spectrum of activity of the selected derivatives.**

42
43 140 Despite all the Bac7(1-16) derivatives having a similar efficacy against *E. coli*, their mode of action
44
45 141 or their spectrum of activity could have changed compared to the wild-type peptide. Initially we
46
47
48 142 verified if Bac7 derivatives still exploited the bacterial transporter SbmA to be fully active ⁵. To do
49
50 143 this, the MIC and minimum bactericidal concentration (MBC) of the Bac7(1-16) derivatives were
51
52 144 determined against the SbmA null mutant *E. coli* strain, BW25113 ΔsbmA . Interestingly, B7-002,
53
54
55 145 and especially B7-004 and B7-005, displayed very little difference (2-4 fold) in MIC and MBC
56
57 146 between the wild-type and ΔsbmA strains (**Table 3**), whereas, by contrast, Bac7(1-16) showed a 16-
58
59
60

1
2
3 147 fold increased MBC in the absence of SbmA. These data suggest that B7-004, B7-005 and partially
4
5 148 B7-002, are almost fully independent of the SbmA transporter for their mode of action.
6
7

8
9 149 Since some pathogens are naturally resistant to Bac7 fragments, most likely because of the
10
11 150 absence of SbmA³, we hypothesized that the new derivatives could be active against bacterial
12
13 151 species that do not express SbmA homologues. Therefore, the Bac7(1-16) derivatives were tested
14
15 152 against reference strains of *Pseudomonas aeruginosa* and *Staphylococcus aureus* (which do not
16
17
18 153 express proteins similar to SbmA) as well as *Klebsiella pneumoniae*, *Acinetobacter baumannii*
19
20 154 which possess an SbmA homologue³. We observed that the same derivatives that killed *E. coli*
21
22 155 despite the absence of the membrane transporter also displayed a broadened spectrum of susceptible
23
24
25 156 species. Interestingly, B7-002, B7-004 and B7-005 gained antimicrobial activity against *P.*
26
27 157 *aeruginosa*; B7-004 and especially B7-005 also inhibited *S. aureus*, two species that are not
28
29 158 susceptible to the unmodified Bac7(1-16). In addition, B7-004 and B7-005 displayed higher
30
31 159 antimicrobial activity against *K. pneumoniae* and *A. baumannii* than Bac7(1-16) (**Table 3**). These
32
33
34 160 results indicate that these new derivatives can affect a wider number of pathogenic species and do
35
36 161 not need the presence of the transporter SbmA. We also tested the efficacy of Bac7(1-16)
37
38 162 derivatives against clinical isolates of pathogenic *E. coli*. Each of the Bac7(1-16) derivatives
39
40
41 163 displayed an MIC of 1 μM against all the strains, with the only exception of the *E. coli* EURL-
42
43 164 VTEC C07 in which the MIC was >64 μM for the unmodified Bac7(1-16) but 2 μM for the tetra-
44
45 165 substituted B7-005 (**Table S2**).
46
47

48 166 **Table 3. MIC and MBC of substituted Bac7 peptides on reference and pathogenic strains.**

49
50
51 167 Results are the median of at least 3 independent experiments (n=3). The unmodified Bac7(1-16)
52
53 168 (wt) was used for comparison.
54
55

Bacteria	B7-derivatives MIC (μM)						B7-derivatives MBC (μM)					
	wt	001	002	003	004	005	wt	001	002	003	004	005
<i>E. coli</i> BW25113*	3	1	1	2	2	2	4	1	8	4	8	4

<i>E. coli</i> BW25113 Δ <i>sbmA</i>	16	12	4	16	3	4	64	32	16	32	4	4
<i>E. coli</i> ATCC 25922*	1	1	1	1.5	1	1	2	2	2	2	2	2
<i>K. pneumoniae</i> ATCC 700603	4	16	2	8	4	2	64	64	16	32	32	8
<i>A. baumannii</i> ATCC 19606	32	32	12	32	32	4	>64	64	24	64	32	8
<i>P. aeruginosa</i> ATCC 27853	>64	>64	>64	>64	64	32	>64	>64	32	>64	64	>64
<i>S. aureus</i> ATCC 25923	>64	>64	>64	>64	32	12	>64	>64	>64	>64	>64	>64

*MIC data on *E. coli* BW25113 and *E. coli* ATCC 25922 were reported here from Table 2 for comparison.

Membrane permeabilizing effect of substituted Bac7(1-16) peptides toward *E. coli* cells.

The low dependency on SbmA displayed by some Bac7(1-16) derivatives indicated that they can cross the membrane using a different mechanism. Indeed, the introduction of additional Arg and Trp residues in the sequence suggests that the peptides may have gained the ability to directly interact with the bacterial membranes. To assess this possibility, propidium iodide (PI) uptake and ONPG/ β -galactosidase assays were performed. The PI-fluorescence associated with *E. coli* BW25113 cells treated with each of the Bac7(1-16) derivatives, evaluated by flow cytometry, was taken as an indicator of the extent of membrane permeabilization (Fig. 2). Similarly, the chromogenic hydrolysis of the ONPG, occurring only if the cytosolic β -galactosidase was unmasked, was taken as indicator that the membrane of *E. coli* ML-35 was damaged (Fig. S2). The bacterial membrane of *E. coli* BW25113 cells appeared unchanged in the presence of the wild-type Bac7(1-16) as well as of the peptides B7-001, -002 and -003. A detectable increase in fluorescence was observed in the presence of 8 μ M and 16 μ M of B7-004 and B7-005. The latter peptide also facilitated PI-uptake appreciably at 4 μ M. These results revealed that B7-004, and especially B7-005, had gained the capability to alter the membrane integrity (Fig. 2). Comparable results were obtained also by the ONPG assay (Fig. S2). The similar trend between the decreased dependency on SbmA and the membrane-perturbing activity of B7-004 and B7-005 suggested that these peptides acquired the capability to interact with the membrane, and perhaps to cross it. However,

the highest PI-fluorescence value detected after the treatment with the two peptides at 16 μM was only $\approx 30\%$ of that measured in the presence of the membranolytic peptide antibiotic colistin at 1 μM . In addition, no increase in fluorescence was induced by any of the peptides at their MICs (1-2 μM , **Table 2**). Overall the weak membranolytic effect of both B7-004 and B7-005 when compared to that of colistin and of other membrane-destroying AMPs (*e.g.* melittin ³¹) suggests that their killing activity is not based on the permeabilization of the bacterial membranes.

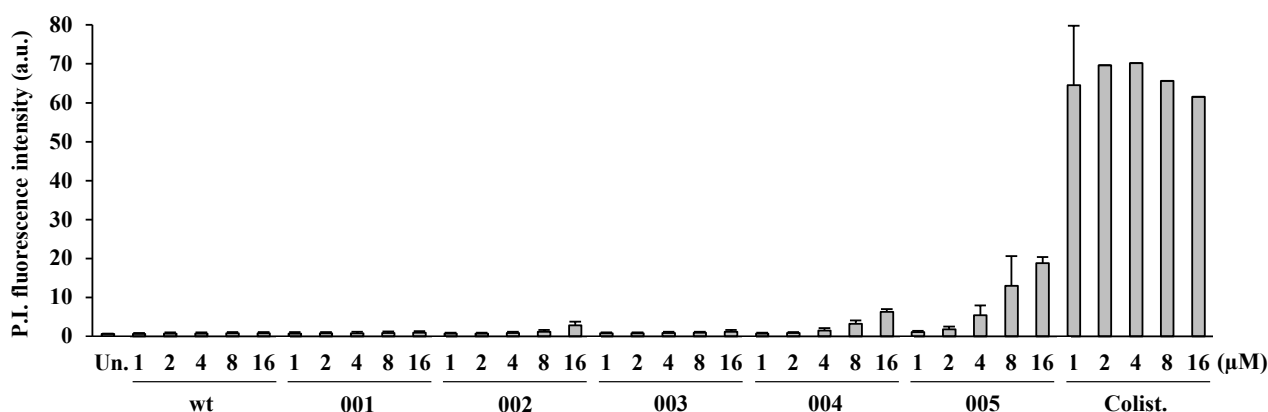


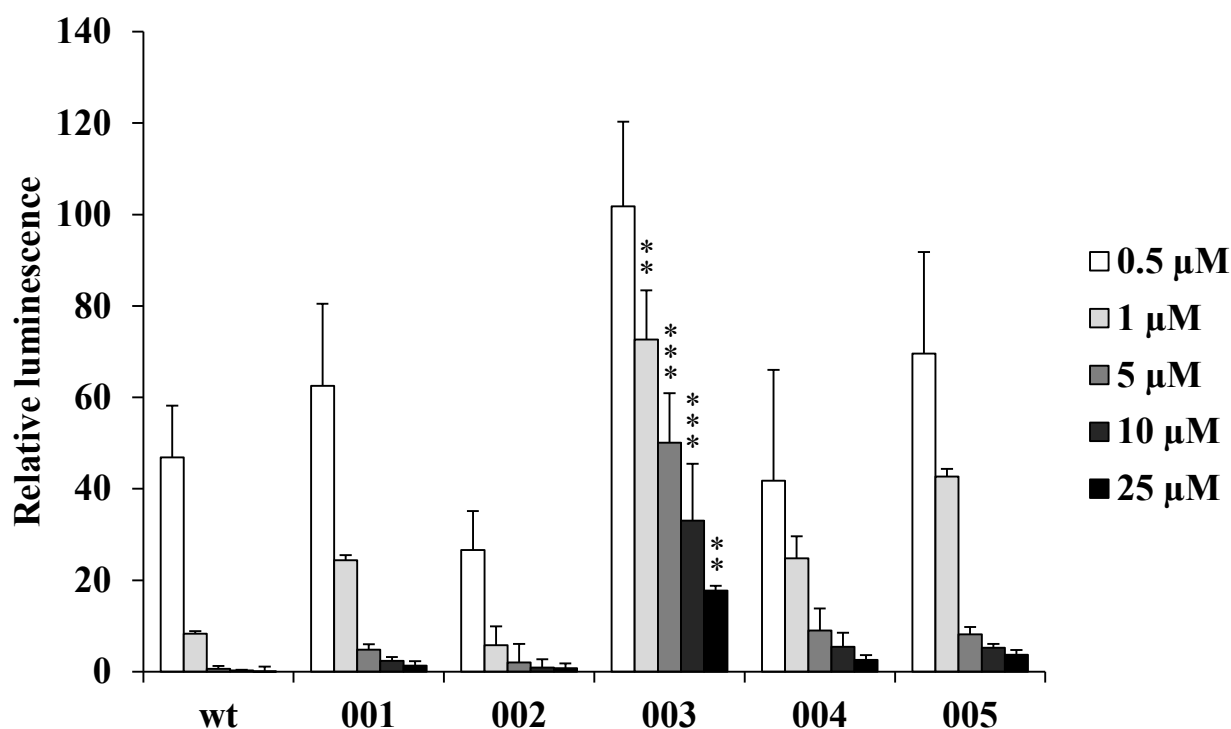
Figure 2. Assessment of *E. coli* BW25113 membranes permeabilization by flow cytometry. The uptake of propidium-iodide (PI) was checked after incubating bacteria for 30 min in the presence of increasing peptides-concentrations evaluating the median fluorescence intensity (MFI) of P.I.-positive bacteria. As a reference for permeabilization, the lytic peptide antibiotic colistin (Colist.) was used. Bacteria were treated with sterile water as untreated control (Un.). Reported data are the average and standard deviation of three independent experiments.

Inhibitory activity of substituted Bac7(1-16) derivatives *in vitro*.

To directly assess if the Bac7(1-16) derivatives maintained the same mechanism of protein synthesis inhibition as the parent peptide ^{3, 11}, we performed *in vitro* transcription/translation assays using *E. coli* lysates. As expected, the unmodified Bac7(1-16) was shown to be an excellent inhibitor of protein synthesis with 90% inhibition observed at 1 μM and complete inhibition at >5

1
2
3 208 μM concentrations (**Fig. 3**). The mono-substituted peptide B7-001 exhibited a slight reduction in
4
5 209 inhibitory activity at 1 μM compared to the wild-type, whereas the effect of the mono-substituted
6
7
8 210 B7-002 was very similar to that of Bac7(1-16). The di-substituted B7-003 was a significantly
9
10 211 weaker inhibitor of the *in vitro* transcription-translation, despite its MIC value being only 2-fold
11
12 212 higher than that of Bac7(1-16) (see **Table 2**). Tri- and tetra-substituted B7-004 and B7-005
13
14
15 213 displayed slightly decreased inhibitory activity compared with that of the wild-type peptide (**Fig. 3**).
16
17

18 214 Overall, only B7-003 clearly reduced its effect on the bacterial translation, without losing
19
20 215 its antibacterial activity on living bacteria. B7-003 was not-permeabilizing (**Fig. 2, Fig. S2**) and still
21
22 216 relied on SbmA to inhibit the bacterial growth (Table 3), suggesting an intracellular mode of action.
23
24
25 217 We hypothesised then that B7-003 could display weak or peculiar interactions with the ribosome,
26
27 218 thereby explaining its dissimilar inhibition of protein synthesis compared to the other derivatives.
28
29
30
31
32
33
34
35
36
37
38
39
40
41
42
43
44
45
46
47
48
49
50
51
52



53 219
54
55
56 220 **Figure 3. Luciferase activity after *in vitro* transcription/translation reactions.** *E. coli* lysates
57
58 221 were treated with increasing concentrations of modified PrAMPs. Results are presented as the
59
60 222 percentage of control samples treated with only RNase free water. Average and standard deviation

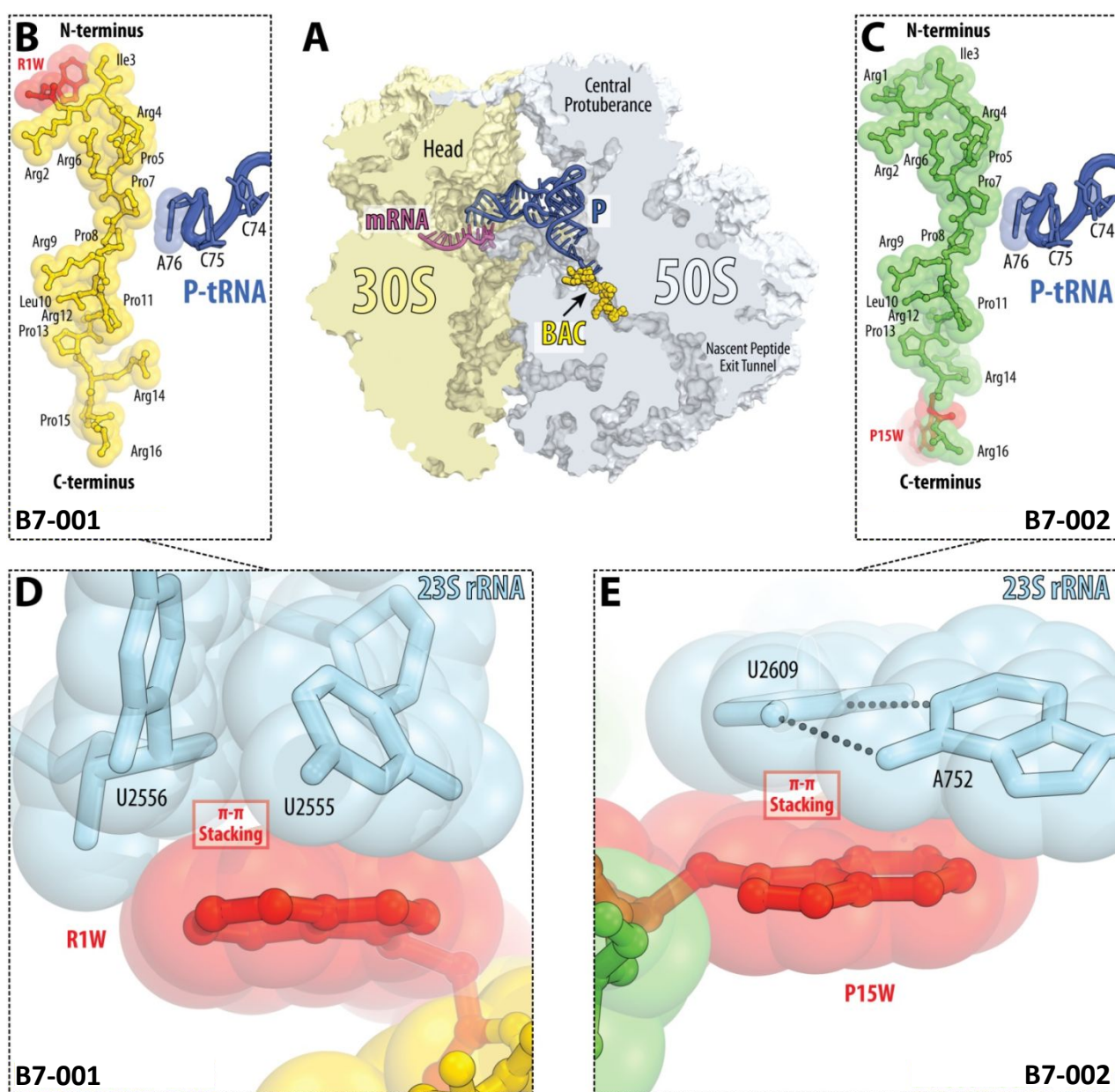
of at least 5 independent experiments (n=5). Student t-test for each concentration of B7-003 VS the same concentration of all the other derivatives, ** = p-value < 0.01, *** = p-value < 0.001.

Crystal structures of Bac7(1-16) derivatives in complex with the 70S ribosome

To understand how the substitutions within mono- and multi-substituted Bac7(1-16) derivatives influence ribosome binding, the structures of Bac7(1-16) derivatives in complex with the *Thermus thermophilus* 70S ribosome were analysed and compared to that of Bac7(1-16)^{11, 13}. We obtained satisfactory electron density maps (**Fig. S3A-D**) and built corresponding structures of B7-001 and B7-002 in complex with the ribosome at 3.0 Å and 3.05 Å resolution, respectively (**Fig. 4 A-C**). The quality of the electron density map allowed the building of molecular models for each of the peptides with the side chains for residues 1-15, with the overall conformation and interactions within the ribosomal tunnel very similar to that reported previously for Bac7(1-16)^{11, 13} (**Fig. S4B-C**). By contrast, despite numerous attempts, we were not able to obtain electron density maps with sufficient detail for the ribosome-bound multi-substituted B7-003, B7-004 and B7-005 peptides. From the few low-resolution datasets, we could infer that all the peptides have the same overall binding site in the nascent peptide exit tunnel within the *T. thermophilus* 70S ribosome (**Fig. S5A-C**), however, the details of their interactions with the ribosome could not be deciphered. This may be due to the increased charge of the multi-substituted peptides that interfered with crystal packing and/or to the weak binding affinity of those peptides to *T. thermophilus* ribosomes.

The side-chain of Arg1 in the Bac7(1-16), formed two hydrogen bonds (H-bonds) with the nucleotides U2555 and C2556 of the 23S rRNA¹¹. Substitution of R1W in B7-001 led to a loss of the H-bonds, suggesting they are not critical for activity. This is consistent with the observation that Bac7(1-16)-derivatives with substitutions of Arg1 to Ala, Gly, or Pro still retained excellent antimicrobial activity (see **Table 1**). Nevertheless, the loss of H-bonding in B7-001 appeared to be compensated for by stacking interactions between the Trp1 and the base of U2555 and the ribose of U2556 (**Fig. 4D**). In the unmodified peptide, Pro15 did not establish any interactions with

1
2
3 248 components of the ribosomal tunnel ¹¹, whereas the substitution of P15W in B7-002 generates
4
5 249 additional stacking interactions between the side-chain of Trp15 and the base-pair between
6
7
8 250 nucleotides A752 and U2609 of the 23S rRNA (**Fig. 4E**). This additional interaction may contribute
9
10 251 to its slightly increased antibacterial activity against *E. coli* BW25113 (see **Table 2**) compared to
11
12 252 the unmodified peptide.



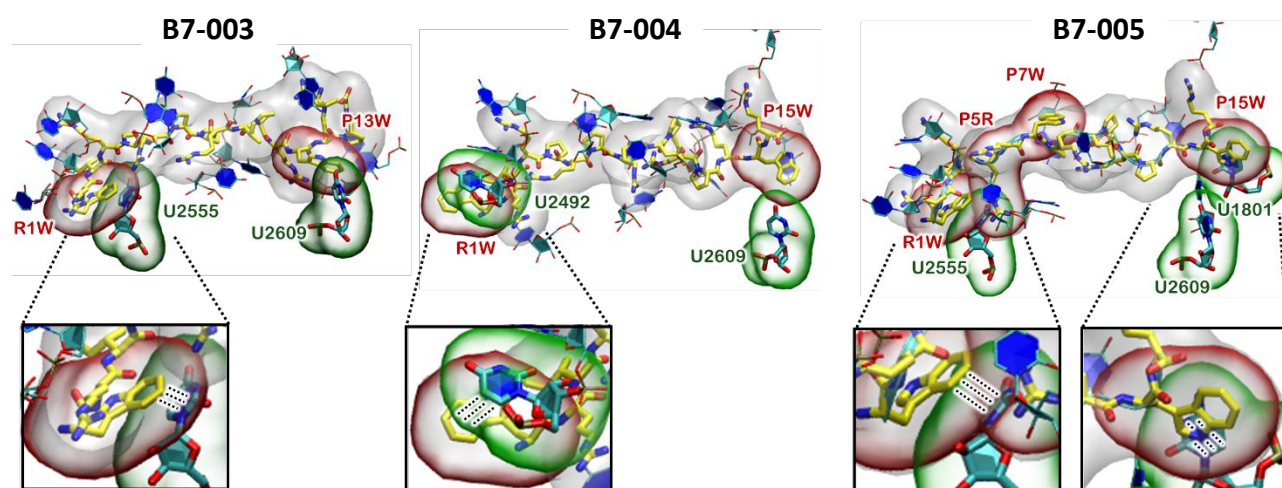
58 255
59
60 256

1
2
3 257 **Figure 4. Structure of B7-001 and B7-002 in complex with the *Tth* 70S ribosome and P-site**
4
5 258 **tRNA. (A)** Overview of the Bac7 binding site (yellow) in the *T. thermophilus* 70S ribosome viewed
6
7
8 259 as a cross-cut through the nascent peptide exit tunnel. The 30S subunit is shown in light yellow, the
9
10 260 50S subunit is in light blue, the mRNA and the P-site tRNA are magenta and dark blue,
11
12 261 respectively. **(B, C)** Close-up views of the B7-001 (yellow, B) and B7-002 (green, C) binding sites
13
14
15 262 relative to the P-site tRNA (dark blue). Note that in the presence of Bac7(1-16)-derivatives,
16
17 263 nucleotide A76 of the P-site tRNA flips out by about 180 degrees into a new conformation, in
18
19 264 which it no longer forms H-bond interactions with A2451 and the A-site substrate that are required
20
21
22 265 for efficient peptide bond formation. **(D, F)** Detailed views of the interactions between the mutated
23
24 266 residues R1W (red, D) in B7-001 (yellow) or P15W (red, E) in B7-002 (green) with the indicated
25
26 267 nucleotides of the 23S rRNA. PDB entry for starting structure: 4Y4P.
27
28
29 268

30
31
32 269 **Molecular dynamics of non-crystalized Bac7(1-16) derivatives in complex with the 70S**
33
34 270 **ribosome**

35
36
37 271 To predict at atomic-level the details of the interactions between the ribosome and the Bac7
38
39 272 derivatives that were not described in detail by X-ray crystallography, cumulative 600 ns-long
40
41
42 273 molecular dynamics simulations of the ribosomal 50S subunit model in explicit water solvent (a
43
44 274 total of 1,350,000 atoms) were performed. The flexibility was measured for all the simulated
45
46 275 peptides by monitoring the Root Mean Square Fluctuation (RMSF) per residue, assuming that low
47
48
49 276 flexibility likely indicates stable binding of the peptide to the ribosome. Models of B7-003, -004
50
51 277 and -005 displayed a RMSF profile similar to that of the original Bac7(1-16) (**Fig. S6**), so they were
52
53 278 predicted to bind the ribosomal exit tunnel similarly to the unmodified peptide. As a control, the
54
55
56 279 Bac7(1-16) derivatives B7-R9G and B7-P13E, showing very poor antimicrobial activity (**Table 1**),
57
58 280 were also simulated and displayed a RMSF profile quite different from that of the unmodified
59
60 281 Bac7(1-16) and the B7-003, -004 and -005 derivatives (**Fig. S6**), pinpointing a remarkably higher

1
2
3 282 flexibility and suggesting poorer binding. The low-resolution data provided by crystallographic
4
5 283 studies were therefore supported and expanded by mapping the interactions of the peptide residues
6
7 284 (**Fig. 5**). In the peptide B7-003, the W13 (substitution P13W) did not interact with the surrounding
8
9
10 285 rRNA nucleobase, most probably due to the structural rearrangement induced by the π -stacking
11
12 286 interaction of W1 with the U2555 residue of the ribosomal tunnel (**Fig. 5**). Similarly, the
13
14 287 substitution R1W appeared to impair the interaction of W15 with U2609, as observed for the
15
16
17 288 peptide B7-004 (**Fig. 5**). The interaction between W15 and surrounding nucleotides was partially
18
19 289 restored in the peptide B7-005 where the interaction between W1 and U2555 was slightly
20
21 290 weakened. This may be due to the rearrangements induced in B7-005 by the substitutions P5R and
22
23
24 291 P7W (**Fig. 5**). This systematic structural analysis delineates how gluing the N-terminus of the
25
26 292 peptide may help anchoring the peptide into the ribosome's tunnel, in line with the structural data
27
28 293 shown above. Conversely, the substitution of further residues may destabilize the π -stacking
29
30 294 interactions established by W1 decreasing the binding affinity of the peptide and its biological
31
32
33 295 effect.
34
35 296
36
37



38
39
40
41
42
43
44
45
46
47
48
49
50
51
52 297
53
54
55 298 **Figure 5. Binding poses of the peptides B7-003, B7-004 and B7-005 (space filling and sticks) as**
56
57 299 **extracted from a cluster analysis of the molecular dynamics simulation trajectories.** For clarity
58
59 300 only the nucleotides of the *T. thermophilus* ribosomal exit tunnel interacting with the peptides are

1
2
3
4
5
6
7
8
9
10
11
12
13
14
15
16
17
18
19
20
21
22
23
24
25
26
27
28
29
30
31
32
33
34
35
36
37
38
39
40
41
42
43
44
45
46
47
48
49
50
51
52
53
54
55
56
57
58
59
60

301 shown and represented as licorice with carbon atoms depicted in yellow (peptide) and cyan
302 (ribosome), while oxygen and nitrogen atoms are displayed in red and blue, respectively. Mutated
303 peptide residues are encircled in red surface, and surrounding interacting RNA nucleotides are
304 highlighted in green surface. Dashed lines depict π -stacking interactions. PDB entry for starting
305 structure: 5F8K.

306

Discussion

Currently, PrAMPs cannot fully address the clinical need for new antimicrobials. Their spectrum of activity is not broad enough for many general applications. Moreover, PrAMPs mainly rely on the non-essential bacterial membrane protein SbmA to be transported into the cell and consequently kill the microorganism. Bacteria can therefore potentially develop resistance against these compounds relatively easily by mutating the transporter. Moreover, the scarce knowledge of the structure-activity relationships that explain ribosome binding and protein synthesis inhibition by these peptides has so far prevented the optimization and rational design of more potent PrAMP-derivatives. The identification of the Bac7(1-16) residues critical for interacting with the ribosome and facilitating the block of the bacterial protein synthesis and growth, is therefore mandatory for any optimization of these peptides.

Here we have shown that the short sequence ${}^{-9}\text{RLP}_{11}$ - is crucial for the inhibitory activity of Bac7(1-16) against *E. coli* protein synthesis and viability (see **Fig.1**). The importance of these residues for the mechanism of action of Bac7(1-16) is supported also by our structural studies. The position of the lateral chains of these residues was almost perfectly superimposable in all the crystals obtained in this study, suggesting that they form crucial interactions with the ribosome (**Fig. S4**). The only substitution in the ${}^{-9}\text{RLP}_{11}$ - region that did not impair the antimicrobial activity of Bac7(1-16) was that with Trp, which was well tolerated also along the whole sequence of Bac7(1-16). In a few cases, the exchange of some single residues of the native peptide with Trp even improved the activity of the peptide (**Table 1**, **Table 2**). A similar effect had been reported also for the derivatives of the mammalian PrAMPs Bac5(1-17)²². The boosting effect of Trp on the activity of mammalian PrAMPs is therefore intriguing also because this amino acid is rarely represented in the known sequence of native mammalian PrAMPs⁴. We recently reported that the Tur1B, a PrAMPs isolated from the dolphin *Tursiops truncatus*, has four Trp residues in its 32 residue-long sequence, however, this peptide did not exhibit a strong inhibitory effect on protein synthesis¹⁶. Other cetacean PrAMPs recently identified from protein sequence databases show a

1
2
3 high number of tryptophans (Sola R., unpublished results), suggesting that introduction of Trp has
4
5 already occurred during evolution.
6
7
8
9

10 The antimicrobial effect and the inhibition of protein synthesis activity observed here
11
12 studying mono- and multi-substituted Bac7(1-16)-derivatives was used to generate a consensus
13
14 sequence highlighting the Bac7(1-16) residues that are essential for the inhibition of the protein
15
16 synthesis (**Fig. 6**). Subsequently, to identify the residues needed by PrAMPs to inhibit the bacterial
17
18 ribosome in a more general context, we extended the consensus to other PrAMPs that are known to
19
20 block the protein synthesis and that were crystalized in the ribosomal exit tunnel, *i.e.* the dolphin-
21
22 derived Tur1A¹⁶ and the insect-derived Onc112¹², Pyrrocoricin and Metalnikowin-1¹¹ (**Fig. 6**).
23
24 The sequences of these peptides were therefore manually aligned using common features, which
25
26 were then combined with the collected functional data to identify the key-residues.
27
28
29
30

31 According to our alignment, the N-terminal residues of Bac7(1-16) and Tur1A, although *per*
32
33 *se* important for the antimicrobial activity of the peptide and for its efficacy on the bacterial protein
34
35 synthesis^{11, 16} did not display any similarity with the sequences of the insect-derived PrAMPs. The
36
37 first aligned residues of the consensus are the positively charged R₆ in mammalian PrAMPs and K₃
38
39 in insect PrAMPs. Most of the Bac7(1-16) residues R₉-R₁₄, shared by Bac7(1-16) derivatives
40
41 effectively inhibiting bacterial growth and protein synthesis, were very conserved also among
42
43 insect-derived PrAMPs (**Fig. 6**). Interestingly, with regard to the R₉ of Bac7(1-16) and its
44
45 derivatives, all the other PrAMPs have a Tyr (Y) in that position, regardless of their mammalian or
46
47 insect origin, (**Fig. 6**). This is reasonable, since the space-filling of the lateral chains of Arg and Tyr
48
49 is quite similar. Both the guanidino group of Arg and the phenolic- group of Tyr are quite bulky
50
51 and planar, allowing similar interactions by π -stacking with the surrounding environment in the
52
53 ribosomal exit tunnel. It is worth noting that the PrAMPs-consensus that we propose is in
54
55 agreement with the results of previous studies on the insect-derived PrAMPs pyrrocoricin³² and
56
57 oncocin³³, since the residues highlighted in the consensus (+XXR/YLPRPRX) have been shown
58
59
60

experimentally to be essential for the antimicrobial effect of these peptides. We believe that the PrAMPs-consensus may be instrumental to design new PrAMP derivatives maintaining a good efficacy in inhibiting the bacterial protein synthesis.

Figure 6. Sequence alignment of Bac7(1-16) derivatives with mammalian and insect PrAMPs binding the ribosomal exit tunnel.

Peptide	Sequence
Bac7(1-16)	RRIRPRPPRLPRPRPR
B7-001	<u>W</u> RIRPRPPRLPRPRPR
B7-002	RRIRPRPPRLPRPR <u>W</u> R
B7-003	<u>W</u> RIRPRPPRLPR <u>W</u> RPR
B7-004	<u>W</u> RIR <u>R</u> RPPRLPRPR <u>W</u> R
B7-005	<u>W</u> RIR <u>R</u> R <u>W</u> PRLPRPR <u>W</u> R
Tur1A	RRIRFRPPYLPRPGRR...
Onc112	VDKPPYLPRRPPPrIYNr-NH ₂
Pyrrhocoricin	VDKGSYLPRTPPRPIYNRN
Metalnikowin-1	VDKPDYRPRRPPNM
PrAMPs consensus	+XX*LPRPRX

The Bac7(1-16) residues substituted in this study are underlined. B7-003, the only Bac7(1-16) derivatives with decreased inhibiting activity toward protein synthesis is highlighted in gray. *indicates R or Y.

Looking then at the antibacterial potential of Bac7(1-16)-derivatives, apparently none of the five peptides was endowed with higher antimicrobial activity against the reference *E. coli* strains used for the screening (**Table 2**). Nevertheless, the derivatives with an increased number of Arg and Trp, B7-004 and especially B7-005, displayed substantial improvements compared to the parent

1
2
3 molecule. They exhibited i) wider spectrum of activity including Gram-positive strains and higher
4
5 activity against Gram-negative, as well as ii) limited dependency on the bacterial transporter SbmA,
6
7 suggesting a distinct mode to enter the bacterial cells.
8
9

10 Both B7-004 and B7-005 remained effective inhibitors of the bacterial protein synthesis, but
11
12 at the same time they acquired the tendency to interact, and to moderately perturb, the bacterial
13
14 membrane as they slightly increased its permeability. The high number of Arg and Trp residues
15
16 could explain this feature, possibly strengthening the interaction of B7-004 and B7-005 with the
17
18 membranes and promoting their passage through the phospholipid bilayer. The reduced dependency
19
20 of B7-004 and B7-005 on SbmA is an important advantage for these molecules because in principle
21
22 it makes more difficult for bacteria to resist to their antimicrobial effects. The mutational
23
24 inactivation of SbmA would indeed not affect the bacterial sensitivity to B7-004 and B7-005,
25
26 differently to what has been observed for other native PrAMPs ^{5, 34}. A strong interaction with the
27
28 membrane is usually accompanied by a reduced selectivity for the target and an increase of
29
30 cytotoxicity ³⁵. By contrast, here we observed that the multi-substituted peptides displayed the same
31
32 high biocompatibility of the native Bac7(1-16).
33
34
35
36
37
38

39 The increased capability of Bac7(1-16) derivatives to alter the membrane permeability may
40
41 explain the broadened spectrum of activity displayed by B7-004 and B7-005 and partially by B7-
42
43 002. The peptides not only increased their bactericidal effects against pathogens sensitive to native
44
45 PrAMPs, such as pathogenic *E. coli* strains, *K. pneumoniae* and *A. baumannii* strains, but also
46
47 gained antimicrobial activity against bacterial species e.g. *P. aeruginosa* and *S. aureus* (**Table 3**)
48
49 which are not susceptible to the unmodified Bac7(1-16)⁴. Indeed, both *P. aeruginosa* and *S. aureus*
50
51 do not express SbmA and are much less sensitive to native PrAMPs than the *Enterobacteriaceae* ¹⁹,
52
53 ²⁰ as the peptides cannot easily penetrate inside their cytosol. Against these pathogens, PrAMPs can
54
55 exert only a moderate antibacterial effect, mainly by membrane destabilization, as observed for
56
57 example for *P. aeruginosa* ³⁶.
58
59
60

Conclusions

In summary, B7-005 combines good antibacterial features with the lack of toxic effects against eukaryotic blood cells at concentrations much above its MIC and MBC against many pathogenic strains and with a valuable antimicrobial effect in the presence of human serum. The tolerance of B7-005 against serum proteases is a further optimistic indication that this peptide could be effective to fight a critical clinical condition, such as bacteraemia, which needs rapid and broad-range antibiotic treatment. This derivative could resist these proteolytic enzymes that represent a big threat for PrAMPs and for AMPs in general ³⁷⁻³⁹. B7-005 overcomes therefore some of the major limits of the native PrAMPs. This peptide gets closer to become a lead compound for a broad-range antimicrobial to be used as a first line of defence against most of the ESKAPE pathogens, considered by the World Health Organization a serious threat for the human health. Moreover, we propose a consensus that could drive the design of new PrAMPs-derivatives preserving their capability to inhibit the protein synthesis.

Experimental section

Peptide synthesis

Peptides libraries were synthesized by automated solid-phase peptide synthesis (SPPS) on a Whatman 50 cellulose membrane using an automated MultiPep RSI peptide (Intavis), adapting the manual synthesis protocol described in ⁴⁰. Briefly, the cellulose membrane (10 cm x 15 cm) was functionalized by overnight incubation in 0.2 M Fmoc-Gly-OH (Aldrich), 0.24 M N,N'-diisopropylcarbodiimide (DIC, Fluka) and 0.4 M N-methylimidazole (NMI, Aldrich) in dimethylformamide (DMF, VWR) before automated synthesis. Subsequently, the glycine was deprotected in 20% piperidine (v/v, Acros Organics) in DMF (20 min + 10 min). Peptide synthesis at discrete spots was performed using 9-fluorenyl-methoxycarbonyl/tert-butyl (Fmoc/tBu) strategy. Fmoc amino acids [Bachem, 0.5 M stock solutions in N-methyl-2-pyrrolidone (NMP, VWR)] were pre-activated with equimolar quantities of 1-hydroxybenzotriazole hydrate (HOBt, Aldrich) and DIC (both 1.1 M stock solutions in NMP) and performed by double coupling procedure (2×10 min) to guarantee higher coupling efficiency at each position of the amino acid sequence. The spotting volumes were 0.8 µl for the first cycle and 0.9 µl for the following cycles. After each amino acid coupling cycle, a 5 min acetic anhydride treatment (5% v/v in DMF, Fluka) was employed to cap unreacted residues. Subsequently, the Fmoc protection group was cleaved using 20% (v/v) piperidine in DMF (2× 5 min). Final cleavage of amino acid side-chain protecting groups was carried out with 25 ml of 90% trifluoroacetic acid (TFA) (Acros Organics), 3% tri-isopropylsilane (TIPS, Acros Organics) and 2% water in dichloromethane (DCM, Acros Organics) for 30 min followed by a 120 min treatment with 25 ml of 50% TFA, 3% TIPS and 2% water in DCM. An overnight incubation in a saturated ammonia gas atmosphere cleaved the peptide amides from the solid support. To determine SPOT synthesis yield and quality, an internally standardized control peptide and individually chosen peptides from that synthesis, were used. Using a one-hole-puncher (Ø=6 mm), individual SPOTs were punched-out, transferred into a sterile 96-well round-bottomed

1
2
3 polypropylene non-treated microtiter plate and dissolved overnight in 200 μ l of sterile water at
4
5 room temperature. Peptides concentration was quantified measuring the absorbance at 280 nm using
6
7 a NanoDrop ND1000 spectrophotometer. The same peptides were then analysed by analytical RP-
8
9 HPLC on a Shim-pack VP-ODS column (120 \AA , 150x4.6 mm, Shimadzu) using a LC2010AHT
10
11 system (Shimadzu). The solvent used were 0.01% (v/v) TFA in H₂O (HPLC-grade, VWR, solvent
12
13 A) and 0.01% (v/v) TFA in acetonitrile (HPLC-grade, VWR, solvent B). A linear gradient of 5% to
14
15 70% of solvent B in 32.5 min with an initial 3 min isocratic equilibration, and a flow rate of
16
17 1 ml/min were used. The purity of the crude control peptides was between 37% and 68%. The
18
19 remaining spots were then excised from the membrane at room temperature, placed in microtiter
20
21 plates and the cleaved peptides resuspended overnight in 200 μ l sterile water, lyophilized and re-
22
23 lyophilized from 200 μ l of 10 mM HCl solution to remove TFA. The peptide pellets were
24
25 resuspended in 50 μ l of sterile water and quantified spectrophotometrically using a Nanodrop2000
26
27 measuring the absorbance at 214 nm spectrophotometer. The molar coefficient at 214 nm of each
28
29 peptide was calculated using the in house program ConCalc using the values reported in ⁴¹.

30
31
32
33
34
35
36 Larger amounts of the best candidates peptides (B7-001 -002 -003 -004 -005) were synthesized by
37
38 solid-phase synthesis using Fmoc-chemistry, purified by reverse-phase HPLC to the final purity
39
40 \geq 95% and controlled by mass spectrometry. These peptides were purchased from NovoPro (China),
41
42 lyophilized three times from 10 mM HCl to remove TFA and quantified as reported above.
43
44
45

46 **Bacterial culture**

47
48
49 The bacterial strains used in this work were *Escherichia coli* BW25113, *E. coli* BW25113 Δ *sbmA*
50
51 (JW0368-1, KEIO collection ⁴²), *E. coli* ML-35, *Klebsiella pneumoniae* ATCC 700603,
52
53 *Acinetobacter baumannii* ATCC 19060, *Staphylococcus aureus* ATCC 25922 and *Pseudomonas*
54
55 *aeruginosa* ATCC 27853. The *E. coli* pathogenic strains (*E. coli* EC1÷6) were generously provided
56
57 by the European Union Reference Laboratory for *E. coli* Department of Food Safety, Nutrition and
58
59 Veterinary Public Health, Istituto Superiore di Sanità, Rome, Italy. All the bacterial strains used in
60

1
2
3 this study were grown overnight at 37°C in Müller-Hinton broth (MHB, Difco) with shaking (140
4 rpm), then, the day after, bacterial cultures were diluted approx. 1:40 in fresh MHB and incubated at
5 37°C with shaking (140 rpm) to mid-log phase, until an optical density at 600 nm ($OD_{600} \approx 0.3$) was
6 reached. 50 µg/ml of kanamycin were added to the medium for *E. coli* BW25113 $\Delta sbmA$.
7
8
9

10 11 12 **Minimum inhibitory concentration determination**

13
14
15 Mid-log bacterial cultures were diluted to 5×10^5 colony forming units (CFU)/ml in MHB. The
16 peptides, diluted in MHB to the concentration of 128 µM, were added to the first wells of a
17 round-bottom 96-wells microtiter plate and serially two-fold diluted in a final volume of 50 µl
18 MHB into successive wells. Subsequently, 50 µl of the bacterial suspension 5×10^5 CFU/ml (see
19 above) was added to each well. This reduced the final bacterial load to 2.5×10^4 CFU/well and
20 halved the peptide concentration in the wells. The same amount of untreated bacteria in MHB
21 was used as bacterial growth-control. 100 µl of MHB was used to control the medium sterility.
22 The plate was sealed with parafilm to minimize evaporation and incubated overnight at 37°C
23 (for approx. 18 hours). The MIC was calculated as the lowest compound concentration
24 preventing visible bacterial growth in the wells. In the case of barely detectable growth in the
25 wells, the OD_{620nm} of the plate was measured using a multi-plate reader Tecan equipped with a
26 Sunrise software. The MIC was then calculated as the well whose OD_{620} was reduced by 99%
27 or more, compared to that of the untreated control.
28
29
30
31
32
33
34
35
36
37
38
39
40
41
42
43
44

45 For the MIC assays in the presence of human serum, 6 anonymous blood samples of healthy
46 donors (generous gift of the Blood Bank of the University Hospital “Ospedale Maggiore” of
47 Trieste, Italy) were pooled. After clotting at room temperature, the cloth was removed by
48 centrifugation (2000 g, 10 min). The serum was filtered using in sequence 0.4 µm and 0.22 µm
49 filters, aliquoted aseptically and stored at -20°C.
50
51
52
53
54
55

56 Data are reported as median of independent experiments repeated three times, or four times in
57 case of uncertain values,
58
59
60

Cell toxicity assay

Cytotoxicity assays were performed by the tetrazolium salts test (MTT), exposing the human cell line of lymphocytes B precursors MEC-1 to peptides, and sterile water as a control at 37°C and 5% CO₂. MEC-1 cells were grown in RPMI (Sigma) + 10% Fetal Bovine Serum (FBS, Sigma) + 2 mM Glutamine (Sigma) + 100 U/ml penicillin (Sigma) + 100 µg/ml streptomycin (Sigma). Cells were then counted and diluted to 2×10⁶ cell/ml. Two-fold serial dilutions of the peptides were prepared in 50 µl of cell growth medium in a 96- flat-bottom microtiter plate (Euroclone), then 10⁵ cells were added to each well in a volume of 50 µl in each well, reaching a final volume of 100 µl. As untreated controls, samples received only sterile water. Following 20 hours of exposure to the compounds, 25 µl of a MTT solution (in sterile PBS) were added to each well to reach a final concentration of 1 mg/ml. After 4 h of incubation at 37°C in the dark, 100 µl of Igepal (Sigma-Aldrich) 10% in 10 mM HCl (w/v) were added to each well, and the plate was incubated overnight at 37°C. After approx. 18 hours, the OD_{570nm} of the wells was measured on a plate-reader spectrophotometer Nanoquant infinite M200pro (Tecan). The peptide cytotoxicity was calculated comparing the OD_{570nm} of the treated samples with that of the untreated control. Data are reported as the average ± standard deviation of three independent experiments in single (n=3) or duplicate (n=6).

Assessment of bacterial membrane integrity

For propidium iodide (PI) uptake assay, mid-log *E. coli* BW25113 cultures prepared as above were diluted to 5×10⁵ colony forming units (CFU)/ml in MHB added with a final concentration of 10 µg/ml PI (Sigma), then incubated at 37°, 200 rpm for 30 min in the presence of 1 µM, 2 µM, 4 µM, 8 µM and 16 µM peptides, or colistin sulphate (Sigma) as a control for membrane permeabilization. As untreated controls, bacterial samples were treated with sterile water only. The uptake of PI was evaluated by flow cytometry performed on MACSQuant Analyzer 10 (Milteny Biotec) equipped with a laser 488 nm to assess the PI fluorescence. Results are expressed as median fluorescent

1
2
3 intensity (MFI) of PI of three independent experiments, collecting for each example 20000 events.
4
5 Data were analysed with FlowLogic software (version 7.2.1, Inivai Technologies). The results are
6
7 the average of three independent experiments.
8
9

10 For ONPG/ β -galactosidase assay, mid-log *E. coli* ML-35 cultures prepared as above were
11
12 centrifuged (2000 g, 10 min.), resuspended in PBS to 10^7 CFU/ml, added with a final concentration
13
14 of 1.5 mM ortho-Nitrophenyl- β -galactoside (ONPG) (Sigma) and incubated at 37°C for 30 min in
15
16 the presence of 1 μ M, 2 μ M, 4 μ M, 8 μ M and 16 μ M peptides, or colistin sulphate (Sigma) as a
17
18 control for membrane permeabilization. As untreated controls, bacterial samples were treated with
19
20 sterile water. The chromogenic hydrolysis of the ONPG, occurring if the cytosolic β -galactosidase
21
22 was unmasked by breaches in the bacterial envelope, was evaluated measuring the optical density
23
24 (OD) at 405 nm in a 96-wells flat-bottom microtiter plate using an Infinite200Pro plate reader
25
26 (Tecan). The blank (absorbance of untreated bacteria) was subtracted to the treated samples. Three
27
28 independent experiments were performed as internal duplicate (n=6).
29
30
31
32
33
34
35
36
37

38 ***In vitro* transcription/translation assay**

39
40
41 *Escherichia coli* lysate-based coupled transcription-translation assays (RTS100, BiotechRabbit)
42
43 were performed as described previously for other PrAMPs^{11, 12, 15, 16, 22, 43}. Briefly, 6 μ l reactions,
44
45 with or without Bac7(1-16) peptide were mixed according to the manufacturer's instructions and
46
47 incubated for 1 h at 30°C with shaking (750 rpm). The reaction was then stop by adding 5 μ l
48
49 kanamycin (50 μ g/ μ l). All samples were diluted with 40 μ l of Luciferase assays substrate (Promega)
50
51 into a white 96-well chimney flat bottom microtiter plate (Greiner). The luminescence was then
52
53 measured using a Tecan Infinite M200 plate reader. The relative values were determined by
54
55 defining the luminescence value of the sample without inhibitor as 100%. All the experiments were
56
57 performed in independent tri-replicates.
58
59
60

Crystallographic structure determination.

All chemicals were from Sigma-Aldrich, except for PEG-20K and MPD, which were purchased from Hampton Research. All solutions were made with ultrapure water and filtered through 0.22 μm membranes before use. *E. coli* tRNA_i^{Met} was kindly provided by Dr. Andrey L. Konevega and stored in water at -80 °C. Short mRNAs were ordered from IDT-DNA (Coralville, IA, USA) and stored in the *Tth* ribosome buffer (5 mM HEPES-KOH pH 7.5, 50 mM KCl, 10 mM NH₄Cl, 10 mM Mg(CH₃COO)₂, 0.6 mM β -mercaptoethanol) at -80 °C.

Ribosome complexes containing mRNA and P-site tRNA_i^{Met} were formed as described previously⁴⁴. Bac7(1-16) variants were added to the pre-formed ribosome complexes to a final concentration of 100 μM prior to crystallization. All *Tth* 70S ribosome complexes were formed in the buffer containing 5 mM HEPES-KOH (pH 7.6), 50 mM KCl, 10 mM NH₄Cl, and 10 mM Mg(CH₃COO)₂, and then crystallized in the buffer containing 100 mM Tris-HCl (pH 7.6), 2.9% (w/v) PEG-20K, 7-12% (v/v) MPD, 100-200 mM arginine, 0.5 mM β -mercaptoethanol. Crystals were grown by the vapor diffusion method in sitting drops at 19°C and stabilized as described previously⁴⁴ with Bac7(1-16)-derivatives being added to the stabilization buffers (100 μM each). Diffraction data were collected using beamline 24ID-C and 24ID-E at the Advanced Photon Source (Argonne National Laboratory, Argonne, IL). A complete dataset for each ribosome complex was collected using 0.979Å wavelength at 100K from multiple regions of the same crystal using 0.3° oscillations. The raw data were integrated and scaled using the XDS software package⁴⁵. All crystals belonged to the primitive orthorhombic space group P2₁2₁2₁ with approximate unit cell dimensions of 210Å x 450Å x 620Å and contained two copies of the 70S ribosome per asymmetric unit. Each structure was solved by molecular replacement using PHASER from the CCP4 program suite⁴⁶. The search model was generated from the previously published structures of *T. thermophilus* 70S ribosome with bound mRNA and tRNAs (PDB entry 4Y4P from⁴⁴). The initial molecular replacement

1
2
3 solutions were refined by rigid-body refinement with the ribosome split into multiple domains,
4 followed by positional and individual B-factor refinement using PHENIX ⁴⁷. Non-crystallographic
5 symmetry restraints were applied to 4 domains of the 30S ribosomal subunit (head, body, spur,
6 helix 44), and 4 domains of the 50S subunit (body, L1-stalk, L10-stalk, C-terminus of the L9
7 protein).

8
9
10 Atomic models for Bac7(1-16) derivatives were generated in COOT using standard *de novo*
11 building of a peptide/protein molecule. The final models of the *T. thermophilus* 70S ribosome in
12 complex with mRNA, initiator tRNA_i^{Met} in the P site, and one of the Bac7(1-16) variants were
13 generated by multiple rounds of model building in COOT ⁴⁸, followed by refinement in PHENIX ⁴⁷.

14 All figures showing atomic models were generated using the PyMol software (www.pymol.org).

15
16 To measure the peptides concentration, the absorbance of 1 mM peptide solutions in *T.*
17 *thermophilus* RB (as estimated from dissolved mass) was measured at 205 and 280 nm against *T.*
18 *thermophilus* RB as blank. Peptide concentrations at 280 nm were calculated using the ProtParam
19 tool on the ExPASy web server⁵⁷. Peptide concentrations at 205 nm were calculated using the
20 Protein Parameter Calculator developed by Anthis and Clore⁵⁸.

21 22 23 24 25 26 27 28 29 30 31 32 33 34 35 36 37 38 39 40 41 42 43 **Molecular dynamics (MD) simulations**

44
45 We built models starting from the Gram-negative eubacteria *T. thermophilus* 70S ribosome crystal
46 structure bound with Bac7(1-16) antimicrobial peptide solved at the average resolution of 2.8 Å
47 (PDB entry 5F8K) ¹¹. This structure comprises several RNAs, and numerous proteins and ions. To
48 study the behaviour of Bac7 within the ribosome exit tunnel, we included in our model the
49 ribosomal 50S subunit comprising 5S and 23S rRNAs, A- and P-tRNAs as well as 10 ribosomal
50 proteins that are in direct contact with rRNA and tRNA, 1101 Mg²⁺, 5 Zn²⁺ and 1 K⁺ ions
51 (Supplementary Figure 6). Other components of 70S ribosome system are located far away from the
52
53
54
55
56
57
58
59
60

1
2
3 ribosome exit tunnel and were not expected to affect Bac7 binding and were thus not included in the
4
5 models. In addition to wt Bac7(1-16), three models of mutant Bac7 derivatives were considered:
6
7 B7-003 (R1W, P13W), B7-004 (R1W, P5R, P15W), B7-005 (R1W, P5R, P7W, P15W). Two
8
9 further peptides endowed with poor antimicrobial effect were also considered as controls, Bac7(1-
10
11 16)R9G and Bac7(1-16)P13E, to have a comparison with molecules not expected to bind the
12
13 ribosome. All mutations were inserted by using the tleap module of Ambergtools 16 ⁴⁹. MD
14
15 simulations were performed with Gromacs2016 software package ⁵⁰. The AMBER-ff12SB force
16
17 field (FF) was employed for proteins ⁵¹, while the ff99+bsc0+χOL3 FF was used for RNAs ⁵² and
18
19 additional modrna08 parameters for modified RNA nucleosides ⁵³ since these are the most validated
20
21 and recommended FFs for protein/RNA systems ⁵⁴. Mg²⁺ ions were described with the non-bonded
22
23 fixed point charge FF due to Åqvist ⁵⁵. Na⁺ and K⁺ ions parameters were taken from Joung and
24
25 Cheatham ⁵⁶ while Zn²⁺ ions were modelled with the cationic dummy atoms approach developed by
26
27 Pang ⁵⁷. The system was embedded in a 10 Å layer of TIP3P ⁵⁸ water molecules leading to a box of
28
29 260 x 220 x 276 Å, containing 1101 Mg²⁺ ions, 4 Zn²⁺, 1 K⁺ and 475 Na⁺ counter ions counting up
30
31 to 1 350 000 atoms. The topologies were built with Ambergtools 16 ⁴⁹ and were subsequently
32
33 converted in a GROMACS2016 format using the software acpype ⁵⁹.
34
35
36
37
38
39
40

41 In all simulations we have used a slow equilibration protocol recommended for protein/RNA MD
42
43 simulations⁵⁴ and used for RNA/protein systems ⁶⁰. Namely, the systems went initially through a
44
45 soft minimization using a steepest descent algorithm with a force convergence criterion set to 1000
46
47 kJ mol⁻¹ nm⁻¹. Then, the models were smoothly annealed from 0 to 300 K with a temperature
48
49 gradient of 50 K every 2 ns and for a total of 12 ns. In this phase, only water molecules and Na⁺
50
51 ions were allowed to move, while the rest was subjected to harmonic position restraints with a force
52
53 constant of 1000 kJ/mol nm². Once the temperature was raised up to 300 K, 20 ns of NPT
54
55 simulations were conducted to stabilize the pressure to 1 bar by coupling the systems to a
56
57
58
59
60

1
2
3 Berendsen barostat ⁶¹, imposing the same restraints used in the heating phase. Temperature control
4
5 at 300 K was achieved by stochastic velocity rescaling thermostat ⁶².
6
7

8
9 Subsequently, the barostat was switched to Parrinello-Rahman ^{63, 64} and the position restraints on
10
11 proteins and RNAs were restricted only to the backbone atoms. These were gradually decreased in
12
13 three consecutive steps of 30, 10, and 10 ns each, during which the force constant was set to 1000,
14
15 250, 50 kJ/mol nm², respectively. Finally, after an attentive equilibration protocol of ~80 ns, all the
16
17 restraints were released and the production runs were performed for ~80 ns (for a total of ~160 ns)
18
19 for each of the subjected models. Productive MD simulations were performed on the canonical
20
21 ensemble (NVT) using periodic boundary conditions. LINCS algorithm ⁶⁵ was used to constrain the
22
23 bonds involving hydrogen atoms and the particle mesh Ewald method ⁶⁶ to account for long-range
24
25 electrostatic interactions with a cutoff of 10 Å. An integration time step of 2 fs was used in all
26
27 simulations. The trajectories were inspected with the VMD software ⁶⁷. All analyses, including root
28
29 mean square fluctuations (RMSF), were done with cpptraj module of Ambertools 16 ⁴⁹ on the
30
31 stripped trajectories without water and counter-ions. All analyses were performed on last 60 ns of
32
33 production phase.
34
35
36
37
38
39
40
41

42 **Supporting information**

43
44
45 Additional figures and tables illustrating analysis of the effect of residue-substitutions on the
46
47 Bac7(1-16) antimicrobial activity, cytotoxicity of resin-synthesised peptides on MEC-1 cells, MIC
48
49 on clinically isolated pathogenic *E. coli* strains, MIC and the MBC of Bac7(1-16) and derivatives
50
51 on *E. coli* ML-35, membrane permeabilization evaluated by ONPG/ β -galactosidase assay on *E. coli*
52
53 ML-35, electron density maps depiction and comparison of ribosome-bound Bac7(1-16) and
54
55 derivatives, molecular dynamics to simulate the binding affinity of peptides to the ribosome, model
56
57 of 50S ribosomal subunit used for molecular dynamics simulation.
58
59
60

Accession numbers

Coordinates and structure factors were deposited in the RCSB Protein Data Bank with accession codes: 6XXX for the *T. thermophilus* 70S ribosome in complex with Bac7-001, mRNA, and P-site tRNA; 6YYY for the *T. thermophilus* 70S ribosome in complex with Bac7-002, mRNA, and P-site tRNA. Authors will release the atomic coordinates and experimental data upon article publication.

Corresponding Author Information

*correspondence should be addressed to Marco Scocchi. Email: mscocchi@units.it. Phone: +39 0405588704

Current Author Addresses

Federica Armas: Singapore MIT Alliance for Research and Technology, 1 CREATE way, 138602, Singapore.

Author Contributions

MM, MS, DW, KH, AM conceived the study; MM, RS, BB, EV, DC, JB, FA, ADS, JB, ES, YP, AM designed and performed the experiments; MM, MS, DW, KH, AM, YP wrote and edited the manuscript; MS supervised the whole project.

Acknowledgments

We thank all members of the D.N. Wilson, M. Scocchi, and Y.S. Polikanov laboratories for valuable suggestions. We thank A. Mankin for important discussions and critical feedback. We thank the staff at NE-CAT beamlines 24ID-C and 24ID-E for help with data collection and freezing of the crystals, especially Drs. K. Rajashankar, M. Capel, F. Murphy, I. Kourinov, A. Lynch, S. Banerjee, D. Neau, J. Schuermann, N. Sukumar, J. Withrow, K. Perry and C. Salbego.

1
2
3 This work is based upon research conducted at the Northeastern Collaborative Access Team
4
5 beamlines, which are funded by the National Institute of General Medical Sciences from the
6
7 National Institutes of Health [P41 GM103403 to NE-CAT]. The Pilatus 6M detector on 24ID-C
8
9 beamline is funded by a NIH-ORIP HEI [S10 RR029205 to NE-CAT]. The Eiger 16M detector on
10
11 24ID-E beamline is funded by a NIH-ORIP HEI grant [S10 OD021527 to NE-CAT]. This research
12
13 used resources of the Advanced Photon Source, a U.S. Department of Energy (DOE) Office of
14
15 Science User Facility operated for the DOE Office of Science by Argonne National Laboratory
16
17 under Contract No. DE-AC02-06CH11357. This work was supported by Illinois State start-up
18
19 funds to Y.S. Polikanov.
20
21
22

23
24 This project was supported by the Deutsche Zentrum für Luft- und Raumfahrt (DLR01K11820 to
25
26 D.N.Wilson) within the “RIBOTARGET” consortium under the frame of JPIAMR. Marco Scocchi
27
28 thanks Area Science Park for supporting with the “Made in Trieste project: research programmes
29
30 among regional public bodies and companies”. Kai Hilpert is thanking the Institute of Infection and
31
32 Immunity for a start-up grant.
33
34

35 36 **Abbreviations**

37
38
39 AMPs, antimicrobial peptides; CFU, colony forming unit; Colist, colistin; DIC, N,N'-
40
41 diisopropylcarbodiimide, FBS, fetal bovine serum; FF, force field; Fmoc/tBu, 9-fluorenyl-
42
43 methoxycarbonyl/tert-butyl; H-bonds, hydrogen bonds; HOBt, hydroxybenzotriazole; IDT-DNA,
44
45 integrated DNA technologies; MBC, minimum bactericidal concentration; MFI median fluorescent
46
47 intensity; MHB, Müller-Hinton broth, MIC, minimum inhibitory concentration; MTT, 3-(4,5-
48
49 dimethylthiazol-2-yl)-2,5-diphenyltetrazolium bromide; NMI, N-methylimidazole; PI, propidium
50
51 iodide; PrAMPs, proline-rich antimicrobial peptides; RLU, relative light units; RMSF, root mean
52
53 square fluctuation, RP-HPLC reversed phase high-performance liquid chromatography; scr,
54
55 scrambled; ser, serum; SPPS, solid-phase peptide synthesis; Un, untreated control; wt, unmodified
56
57
58
59
60

1
2
3 peptide; PEG-20K, poly(ethylene glycol) M_n 20000; MPD, 2-methyl-2,4-pentanediol; NVT, number
4
5 volume temperature.
6
7
8
9
10
11
12
13
14
15
16
17
18
19
20
21
22
23
24
25
26
27
28
29
30
31
32
33
34
35
36
37
38
39
40
41
42
43
44
45
46
47
48
49
50
51
52
53
54
55
56
57
58
59
60

References

1. Ventola, C. L. The antibiotic resistance crisis: part 1: causes and threats. *P T* **2015**, *40*, 277-283.
2. Mishra, B.; Reiling, S.; Zarena, D.; Wang, G. S. Host defense antimicrobial peptides as antibiotics: design and application strategies. *Curr Opin Chem Biol* **2017**, *38*, 87-96.
3. Graf, M.; Mardirossian, M.; Nguyen, F.; Seefeldt, A. C.; Guichard, G.; Scocchi, M.; Innis, C. A.; Wilson, D. N. Proline-rich antimicrobial peptides targeting protein synthesis. *Nat Prod Rep* **2017**, *34*, 702-711.
4. Scocchi, M.; Tossi, A.; Gennaro, R. Proline-rich antimicrobial peptides: converging to a non-lytic mechanism of action. *Cell Mol Life Sci* **2011**, *68*, 2317-2330.
5. Mattiuzzo, M.; Bandiera, A.; Gennaro, R.; Benincasa, M.; Pacor, S.; Antcheva, N.; Scocchi, M. Role of the *Escherichia coli* SbmA in the antimicrobial activity of proline-rich peptides. *Mol Microbiol* **2007**, *66*, 151-163.
6. Paulsen, V. S.; Mardirossian, M.; Blencke, H. M.; Benincasa, M.; Runti, G.; Nepa, M.; Haug, T.; Stensvag, K.; Scocchi, M. Inner membrane proteins YgdD and SbmA are required for the complete susceptibility of *Escherichia coli* to the proline-rich antimicrobial peptide arasin 1(1-25). *Microbiology* **2016**, *162*, 601-609.
7. Krizsan, A.; Knappe, D.; Hoffmann, R. Influence of the yjiL-mdtM gene cluster on the antibacterial activity of proline-rich antimicrobial peptides overcoming *Escherichia coli* resistance induced by the missing SbmA transporter system. *Antimicrob Agents Chemother* **2015**, *59*, 5992-5998.

- 1
2
3 8. Krizsan, A.; Volke, D.; Weinert, S.; Strater, N.; Knappe, D.; Hoffmann, R. Insect-derived
4 proline-rich antimicrobial peptides kill bacteria by inhibiting bacterial protein translation at the 70S
5 ribosome. *Angew Chem Int Ed Engl* **2014**, 53, 12236-12239.
6
7
8
9
10
11 9. Mardirossian, M.; Grzela, R.; Giglione, C.; Meinel, T.; Gennaro, R.; Mergaert, P.; Scocchi,
12 M. The host antimicrobial peptide Bac71-35 binds to bacterial ribosomal proteins and inhibits
13 protein synthesis. *Chem Biol* **2014**, 21, 1639-1647.
14
15
16
17
18
19 10. Taniguchi, M.; Ochiai, A.; Kondo, H.; Fukuda, S.; Ishiyama, Y.; Saitoh, E.; Kato, T.;
20 Tanaka, T. Pyrrocoricin, a proline-rich antimicrobial peptide derived from insect, inhibits the
21 translation process in the cell-free *Escherichia coli* protein synthesis system. *J Biosci Bioeng* **2016**,
22 121, 591-598.
23
24
25
26
27
28
29 11. Seefeldt, A. C.; Graf, M.; Perebaskine, N.; Nguyen, F.; Arenz, S.; Mardirossian, M.;
30 Scocchi, M.; Wilson, D. N.; Innis, C. A. Structure of the mammalian antimicrobial peptide Bac7(1-
31 16) bound within the exit tunnel of a bacterial ribosome. *Nucleic Acids Res* **2016**, 44, 2429-2438.
32
33
34
35
36
37 12. Seefeldt, A. C.; Nguyen, F.; Antunes, S.; Perebaskine, N.; Graf, M.; Arenz, S.; Inampudi, K.
38 K.; Douat, C.; Guichard, G.; Wilson, D. N.; Innis, C. A. The proline-rich antimicrobial peptide
39 Onc112 inhibits translation by blocking and destabilizing the initiation complex. *Nat Struct Mol*
40 *Biol* **2015**, 22, 470-475.
41
42
43
44
45
46
47 13. Gagnon, M. G.; Roy, R. N.; Lomakin, I. B.; Florin, T.; Mankin, A. S.; Steitz, T. A.
48 Structures of proline-rich peptides bound to the ribosome reveal a common mechanism of protein
49 synthesis inhibition. *Nucleic Acids Res* **2016**, 44, 2439-2450.
50
51
52
53
54
55 14. Roy, R. N.; Lomakin, I. B.; Gagnon, M. G.; Steitz, T. A. The mechanism of inhibition of
56 protein synthesis by the proline-rich peptide oncocin. *Nat Struct Mol Biol* **2015**, 22, 466-469.
57
58
59
60

- 1
2
3 15. Mardirossian, M.; Barriere, Q.; Timchenko, T.; Muller, C.; Pacor, S.; Mergaert, P.; Scocchi,
4 M.; Wilson, D. N. fragments of the nonlytic proline-rich antimicrobial peptide Bac5 kill
5 *Escherichia coli* cells by inhibiting protein synthesis. *Antimicrob Agents Chemother* **2018**, 62,
6 e00534-18.
7
8
9
10
11
12
13 16. Mardirossian, M.; Perebaskine, N.; Benincasa, M.; Gambato, S.; Hofmann, S.; Huter, P.;
14 Muller, C.; Hilpert, K.; Innis, C. A.; Tossi, A.; Wilson, D. N. The dolphin proline-rich antimicrobial
15 peptide Tur1A inhibits protein synthesis by targeting the bacterial ribosome. *Cell Chem Biol* **2018**,
16 25, 530-539.
17
18
19
20
21
22
23 17. Florin, T.; Maracci, C.; Graf, M.; Karki, P.; Klepacki, D.; Berninghausen, O.; Beckmann,
24 R.; Vazquez-Laslop, N.; Wilson, D. N.; Rodnina, M. V.; Mankin, A. S. An antimicrobial peptide
25 that inhibits translation by trapping release factors on the ribosome. *Nat Struct Mol Biol* **2017**, 24,
26 752-757.
27
28
29
30
31
32
33 18. Matsumoto, K.; Yamazaki, K.; Kawakami, S.; Miyoshi, D.; Ooi, T.; Hashimoto, S.;
34 Taguchi, S. *In vivo* target exploration of apidaecin based on Acquired Resistance induced by Gene
35 Overexpression (ARGO assay). *Sci Rep* **2017**, 7, Article12136.
36
37
38
39
40
41 19. Bluhm, M. E.; Knappe, D.; Hoffmann, R. Structure-activity relationship study using peptide
42 arrays to optimize Api137 for an increased antimicrobial activity against *Pseudomonas aeruginosa*.
43 *Eur J Med Chem* **2015**, 103, 574-582.
44
45
46
47
48
49 20. Knappe, D.; Ruden, S.; Langanke, S.; Tikko, T.; Ritzer, J.; Mikut, R.; Martin, L. L.;
50 Hoffmann, R.; Hilpert, K. Optimization of oncocin for antibacterial activity using a SPOT synthesis
51 approach: extending the pathogen spectrum to *Staphylococcus aureus*. *Amino Acids* **2016**, 48, 269-
52 280.
53
54
55
56
57
58
59
60

- 1
2
3 21. Guida, F.; Benincasa, M.; Zahariev, S.; Scocchi, M.; Berti, F.; Gennaro, R.; Tossi, A. Effect
4 of size and N-terminal residue characteristics on bacterial cell penetration and antibacterial activity
5 of the proline-rich peptide Bac7. *J Med Chem* **2015**, 58, 1195-1204.
6
7
8
9
10
11 22. Mardirossian, M.; Sola, R.; Beckert, B.; Collis, D. W. P.; Di Stasi, A.; Armas, F.; Hilpert,
12 K.; Wilson, D. N.; Scocchi, M. Proline-rich peptides with improved antimicrobial activity against
13 *E. coli*, *K. Pneumoniae*, and *A. Baumannii*. *ChemMedChem* **2019**, 14, 2025-2033.
14
15
16
17
18 23. Mardirossian, M.; Sola, R.; Degasperi, M.; Scocchi, M. Search for shorter portions of the
19 proline-rich antimicrobial peptide fragment Bac5(1-25) that retain antimicrobial activity by
20 blocking protein synthesis. *ChemMedChem* **2019**, 14, 343-348.
21
22
23
24
25
26 24. Knappe, D.; Stegemann, C.; Nimptsch, A.; Kolobov, A., Jr.; Korableva, E.; Shamova, O.;
27 Kokryakov, V. N.; Hoffmann, R. Chemical modifications of short antimicrobial peptides from
28 insects and vertebrates to fight multi-drug resistant bacteria. *Adv Exp Med Biol* **2009**, 611, 395-396.
29
30
31
32
33
34 25. Lopez-Perez, P. M.; Grimsey, E.; Bourne, L.; Mikut, R.; Hilpert, K. Screening and
35 optimizing antimicrobial peptides by using SPOT-Synthesis. *Front Chem* **2017**, 5, Article 25.
36
37
38
39 26. Lai, P. K.; Geldart, K.; Ritter, S.; Kaznessis, Y. N.; Hackel, B. J. Systematic mutagenesis of
40 oncocin reveals enhanced activity and insights into the mechanisms of antimicrobial activity. *Mol*
41 *Syst Des Eng* **2018**, 3, 930-941.
42
43
44
45
46
47 27. Benincasa, M.; Scocchi, M.; Podda, E.; Skerlavaj, B.; Dolzani, L.; Gennaro, R.
48 Antimicrobial activity of Bac7 fragments against drug-resistant clinical isolates. *Peptides* **2004**, 25,
49 2055-2061.
50
51
52
53
54 28. Lai, P. K.; Tresnak, D. T.; Hackel, B. J. Identification and elucidation of proline-rich
55 antimicrobial peptides with enhanced potency and delivery. *Biotechnol Bioeng* **2019**, 116, 2439-
56 2450.
57
58
59
60

- 1
2
3 29. Casalino, L.; Palermo, G.; Abdurakhmonova, N.; Rothlisberger, U.; Magistrato, A.
4
5 Development of site-specific Mg(2+)-RNA force field parameters: a dream or reality? Guidelines
6
7 from combined molecular dynamics and quantum mechanics simulations. *J Chem Theory Comput*
8
9 **2017**, 13, 340-352.
10
11
12
13 30. Casalino, L.; Palermo, G.; Rothlisberger, U.; Magistrato, A. Who activates the nucleophile
14
15 in ribozyme catalysis? An answer from the splicing mechanism of group II introns. *J Am Chem Soc*
16
17 **2016**, 138, 10374-10377.
18
19
20
21 31. Lee, M. T.; Sun, T. L.; Hung, W. C.; Huang, H. W. Process of inducing pores in membranes
22
23 by melittin. *Proc Natl Acad Sci U S A* **2013**, 110, 14243-14248.
24
25
26
27 32. Kragol, G.; Hoffmann, R.; Chattergoon, M. A.; Lovas, S.; Cudic, M.; Bulet, P.; Condie, B.
28
29 A.; Rosengren, K. J.; Montaner, L. J.; Otvos, L., Jr. Identification of crucial residues for the
30
31 antibacterial activity of the proline-rich peptide, pyrrocoricin. *Eur J Biochem* **2002**, 269, 4226-
32
33 4237.
34
35
36
37 33. Knappe, D.; Zahn, M.; Sauer, U.; Schiffer, G.; Strater, N.; Hoffmann, R. Rational design of
38
39 oncocin derivatives with superior protease stabilities and antibacterial activities based on the high-
40
41 resolution structure of the oncocin-DnaK complex. *Chembiochem* **2011**, 12, 874-876.
42
43
44
45 34. Narayanan, S.; Modak, J. K.; Ryan, C. S.; Garcia-Bustos, J.; Davies, J. K.; Roujeinikova, A.
46
47 Mechanism of Escherichia coli Resistance to Pyrrocoricin. *Antimicrob Agents Chemother* **2014**,
48
49 58, 2754-2762.
50
51
52
53 35. Brunetti, J.; Falciani, C.; Roscia, G.; Pollini, S.; Bindi, S.; Scali, S.; Arrieta, U. C.; Gomez-
54
55 Vallejo, V.; Quercini, L.; Ibba, E.; Prato, M.; Rossolini, G. M.; Llop, J.; Bracci, L.; Pini, A. *In vitro*
56
57 and *in vivo* efficacy, toxicity, bio-distribution and resistance selection of a novel antibacterial drug
58
59 candidate. *Sci Rep* **2016**, 6, Article 26077.
60

- 1
2
3 36. Runti, G.; Benincasa, M.; Giuffrida, G.; Devescovi, G.; Venturi, V.; Gennaro, R.; Scocchi,
4
5 M. The mechanism of killing by the proline-rich peptide Bac7(1-35) against clinical strains of
6
7 *Pseudomonas aeruginosa* differs from that against other gram-negative bacteria. *Antimicrob Agents*
8
9 *Chemother* **2017**, 61, e01660-16.
- 10
11
12
13 37. Moncla, B. J.; Pryke, K.; Rohan, L. C.; Graebing, P. W. Degradation of naturally occurring
14
15 and engineered antimicrobial peptides by proteases. *Adv Biosci Biotechnol* **2011**, 2, 404-408.
- 16
17
18 38. Mattiuzzo, M.; De Gobba, C.; Runti, G.; Mardirossian, M.; Bandiera, A.; Gennaro, R.;
19
20 Scocchi, M. Proteolytic activity of *Escherichia coli* oligopeptidase B against proline-rich
21
22 antimicrobial peptides. *J Microbiol Biotechnol* **2014**, 24, 160-167.
- 23
24
25
26 39. Mardirossian, M.; Pompilio, A.; Crocetta, V.; De Nicola, S.; Guida, F.; Degasperi, M.;
27
28 Gennaro, R.; Di Bonaventura, G.; Scocchi, M. *In vitro* and *in vivo* evaluation of BMAP-derived
29
30 peptides for the treatment of cystic fibrosis-related pulmonary infections. *Amino Acids* **2016**, 48,
31
32 2253-2260.
- 33
34
35
36 40. Hilpert, K.; Winkler, D. F.; Hancock, R. E. Peptide arrays on cellulose support: SPOT
37
38 synthesis, a time and cost efficient method for synthesis of large numbers of peptides in a parallel
39
40 and addressable fashion. *Nat Protoc* **2007**, 2, 1333-13349.
- 41
42
43
44 41. Kuipers, B. J. H.; Gruppen, H. Prediction of molar extinction coefficients of proteins and
45
46 peptides using UV absorption of the constituent amino acids at 214 nm to enable quantitative
47
48 reverse phase high-performance liquid chromatography-mass spectrometry analysis. *J Agr Food*
49
50 *Chem* **2007**, 55, 5445-5451.
- 51
52
53
54 42. Baba, T.; Ara, T.; Hasegawa, M.; Takai, Y.; Okumura, Y.; Baba, M.; Datsenko, K. A.;
55
56 Tomita, M.; Wanner, B. L.; Mori, H. Construction of *Escherichia coli* K-12 in-frame, single-gene
57
58 knockout mutants: the Keio collection. *Mol Syst Biol* **2006**, 2, Article 2006.0008.
- 59
60

- 1
2
3 43. Leoni, G.; De Poli, A.; Mardirossian, M.; Gambato, S.; Florian, F.; Venier, P.; Wilson, D.
4
5 N.; Tossi, A.; Pallavicini, A.; Gerdol, M. Myticalins: A novel multigenic family of linear, cationic
6
7 antimicrobial peptides from Marine Mussels (*Mytilus spp.*). *Mar Drugs* **2017**, 15, Article 261.
8
9
10
11 44. Polikanov, Y. S.; Melnikov, S. V.; Soll, D.; Steitz, T. A. Structural insights into the role of
12
13 rRNA modifications in protein synthesis and ribosome assembly. *Nat Struct Mol Biol* **2015**, 22,
14
15 342-344.
16
17
18 45. Kabsch, W. Xds. *Acta Crystallogr D* **2010**, 66, 125-132.
19
20
21 46. McCoy, A. J.; Grosse-Kunstleve, R. W.; Adams, P. D.; Winn, M. D.; Storoni, L. C.; Read,
22
23 R. J. Phaser crystallographic software. *J Appl Crystallogr* **2007**, 40, 658-674.
24
25
26
27 47. Adams, P. D.; Afonine, P. V.; Bunkoczi, G.; Chen, V. B.; Davis, I. W.; Echols, N.; Headd,
28
29 J. J.; Hung, L. W.; Kapral, G. J.; Grosse-Kunstleve, R. W.; McCoy, A. J.; Moriarty, N. W.; Oeffner,
30
31 R.; Read, R. J.; Richardson, D. C.; Richardson, J. S.; Terwilliger, T. C.; Zwart, P. H. PHENIX: a
32
33 comprehensive Python-based system for macromolecular structure solution. *Acta Crystallogr D*
34
35 *Biol Crystallogr* **2010**, 66, 213-221.
36
37
38
39 48. Emsley, P.; Cowtan, K. Coot: model-building tools for molecular graphics. *Acta Crystallogr*
40
41 *D Biol Crystallogr* **2004**, 60, 2126-2132.
42
43
44
45 49. Case, D.; A., Darden, T., Cheatham, T., E., Simmerling, C.; Wang, J.; Duke, R., E.; Luo, R.;
46
47 Walker, R., C.; Zhang, W., Merz, K., M. AMBER 2016, *University of California, San Francisco*
48
49 **2016**.
50
51
52 50. Van Der Spoel, D.; Lindahl, E.; Hess, B.; Groenhof, G.; Mark, A.,E.; Berendsen, H.,J
53
54 GROMACS: fast, flexible, and free. *J Comput Chem.* **2007**, 26, 701-718.
55
56
57
58
59
60

- 1
2
3 51. Maier, J. A.; Martinez, C.; Kasavajhala, K.; Wickstrom, L.; Hauser, K. E.; Simmerling, C.
4
5 ff14SB: improving the accuracy of protein side chain and backbone parameters from ff99SB.
6
7 *Journal of Chemical Theory and Computation* **2015**, 11, 3696-3713.
8
9
10 52. Perez, A.; Marchan, I.; Svozil, D.; Sponer, J.; Cheatham, T. E., 3rd; Laughton, C. A.;
11
12 Orozco, M. Refinement of the AMBER force field for nucleic acids: improving the description of
13
14 alpha/gamma conformers. *Biophys J* **2007**, 92, 3817-3829.
15
16
17 53. Aduri, R.; Psciuk, B. T.; Saro, P.; Taniga, H.; Schlegel, H. B.; SantaLucia, J. AMBER force
18
19 field parameters for the naturally occurring modified nucleosides in RNA. *J Chem Theory Comput*
20
21 **2007**, 3, 1464-1475.
22
23
24 54. Sponer, J.; Krepl, M.; Banáš, P.; Kührová, P.; Zgarbová, M.; Jurečka, P.; Havrila, M.;
25
26 Otyepka, M. How to understand atomistic molecular dynamics simulations of RNA and protein-
27
28 RNA complexes? *Wiley Interdiscip. Rev. RNA* **2017**, 2, e1405.
29
30
31
32
33 55. Aqvist, J. Ion water interaction potentials derived from free-energy perturbation simulations.
34
35 *J. Phys. Chem.* **1990**, 94, 8021-8024.
36
37
38
39
40
41 56. Joung, I.S.; Cheatham, T.E. Determination of alkali and halide monovalent ion parameters
42
43 for use in explicitly solvated biomolecular simulations. *J Phys. Chem. B* **2008**, 112, 30, 9020-9041
44
45
46
47
48 57. Pang, Y.P. Novel zinc protein molecular dynamics simulations: Steps toward
49
50 antiangiogenesis for cancer treatment. *J Mol Model.* **1999**, 5, 196-202.
51
52
53
54
55 58. Jorgensen, W.L.; Chandrasekhar, J. and Madura, J.D. Comparison of simple potential
56
57 functions for simulating liquid water. *J Chem Phys.* **1983**, 79, 926-935.
58
59
60

- 1
2
3 59 Sousa da Silva, A.W.; Vranken, W.F. ACPYPE - AnteChamber PYthon Parser interface.
4
5 *BMC ResNotes*. **2012**, 5, Article 367.
6
7
8
9
10
11 60. Casalino, L.; Palermo, G.; Spinello, A.; Rothlisberger, U.; Magistrato, A. All-atom
12 simulations disentangle the functional dynamics underlying gene maturation in the intron lariat
13 spliceosome. *P Natl Acad Sci USA* **2018**, 115, 6584-6589.
14
15
16
17
18
19 61. Berendsen, H.J.C.; Postma, J., P.; M., van Gunsteren, W., F.; Di Nola, A.; Haak, J., R.
20 Molecular-Dynamics with Coupling to an External Bath. *J Chem Phys*. **1984**, 81, 3684-3690.
21
22
23
24
25
26
27 62. Bussi, G.; Donadio, D.; Parrinello, M. Canonical sampling through velocity rescaling. *J*
28 *Cheml Phys*. **2007**, 126, Article 014101.
29
30
31
32
33
34 63. Parrinello, M.; Rahman, A. Crystal-structure and pair potentials - a molecular-dynamics
35 study. *Phys Rev Lett*, **1980**, 45, 1196-1199.
36
37
38
39
40
41 64. Parrinello, M.; Rahman, A. Polymorphic transitions in single-crystals - a new molecular-
42 dynamics method. *J App Phys*. **1981**, 52, 7182-7190.
43
44
45
46
47 65. Hess, B.; Bekker, H.; Berendsen H.J.; Fraaije J.E. LINCS: A linear constraint solver for
48 molecular simulations. *J Comput Chem*. **1997**, 18, 1463-1472.
49
50
51
52
53
54 66. Darden, T.; York, D.; Pedersen, L. Particle Mesh Ewald - an N.Log(N) method for ewald
55 sums in large systems. *J Cheml Phys*, **1993**, 98, 10089-10092.
56
57
58
59
60

1
2
3 67. Humphrey, W.; A. Dalke; K. Schulten. VMD: Visual molecular dynamics. *Journal of*
4
5 *Molecular Graphics and Modelling*. 1996, 14. 33-38.
6
7
8
9
10
11

12 Graphical table of content

13
14
15
16
17
18

